Technical Report

TR-10-64

Modelling of erosion of bentonite gel by gel/sol flow

Luis Moreno, Ivars Neretnieks, Longcheng Liu

Chemical Engineering and Technology
Royal Institute of Technology

November 2010

Svensk Kärnbränslehantering AB
Swedish Nuclear Fuel
and Waste Management Co

Box 250, SE-101 24 Stockholm
Phone +46 8 459 84 00

ISSN 1404-0344
SKB TR-10-64

Modelling of erosion of bentonite gel by gel/sol flow

Luis Moreno, Ivars Neretnieks, Longcheng Liu

Chemical Engineering and Technology
Royal Institute of Technology

November 2010

Keywords: Smectite gel, Viscosity, Flow, Erosion, Diffusion.

Abstract

Bentonite gel that expands into a fracture with seeping water will release colloids into low ionic strength waters. In addition the gel/sol can itself slowly flow downstream when it has reached a low particle concentration sufficient to decrease the viscosity to allow flow. The erosion due to the combined effects of particle diffusion and gel/sol flow is modelled for a thin fracture into which the gel expands influenced by various forces between and on particles. Some of the forces such as the electrical double layer force and viscous force are strongly influenced by the ionic strength of the pore water. Changes in the ionic strength due to diffusion and dilution of ions in the expanding clay are modelled simultaneously with the gel expansion, flow of gel and colloid release to the seeping water. The model includes description of flow of the seeping fluid, which gradually turns from pure water to sol to more dense gel as the bentonite source is approached, expansion of the gel/sol and colloid release and flow and diffusion of ions in the system. The coupled models are solved using a numerical code.

Sammanfattning

Bentonitgel som expanderar ut i en spricka med sipprande watten lösgör kolloider till vatten med låg jonstyrka. Bentonitgelen övergår gradvis i sol. Denna gel/sol kan sakta röra sig nedströms när partikelkoncentrationen är så låg att gel/solens viskositet tillåter strömning. Erosion genom den kombinerade effekten av partikeldiffusion och gel/sol strömning i tunna sprickor har modellerats där gelen expanderar ut i en spricka i vilken det strömmar vatten som får gel/solen att strömma och där diffusion transporterar partiklarna längre och längre ut i det sipprande vattnet. Partikeldiffusionen och gelexpansionen påverkas av ett antal olika krafter som verkar på och mellan partiklarna. Såväl repulsionen mellan de elektriskt laddade partiklarna och gel/solens viskositet påverkas starkt av vattnets jonstyrka. Denna i sin tur påverkas av jonernas diffusion i gelen från depositionshålet ut mot det sipprande vattnet. Denna process modelleras samtidigt med gel/sol transporten. Modellen innefattar en beskrivning av hur partiklarna i gelen expanderar ut från källan, hur gel/solen strömmar, hur den lösgör kolloidala partiklar till det sipprande vattnet och hur joner diffunderar och strömmar i och med gel/solen. Dessa kopplade processer modelleras och ekvationerna löses med numeriska metoder.

Executive summary

Bentonite intrusion into a fracture intersecting the canister deposition hole is modelled. The model describes the expansion of the bentonite within the fracture (Liu et al. 2009a). It accounts for the repulsive electrostatic double-layer forces, the attractive van der Waals forces and friction forces between the particles and the water. The model also takes into account the diffusion of the colloid particles in the smectite sol. Diffusion of a counterion, sodium, is accounted for as this strongly influences the double layer force and the viscosity of the gel/sol. The gel/sol is considered to be a fluid with a varying viscosity that is strongly dependent on the bentonite volume fraction in the gel and the sodium concentration in the water.

Two different geometries were modelled; a rectangular and a cylindrical. The rectangular geometry was used to gain experience with the processes and mechanisms and how they interact since the cylindrical geometry was somewhat less stable numerically and more time consuming. In the rectangular geometry a fracture 1 metre long in the flow direction was modelled. In both geometries the fracture size was selected sufficiently large to ensure that the water velocity, near the distant border was nearly the same as the approaching water velocity and that the smectite concentration there was vanishingly small.

It was found that the velocity of the fluid drops considerably where the bentonite volume fraction is larger than 1–2%. This is due to the strong increase in viscosity with increasing bentonite volume fraction.

The loss of smectite by the slowly flowing fluid was found to be proportional to the square root of the seeping water velocity for the rectangular geometry. For the cylindrical geometry, the dependence is somewhat lower (exponent about 0.4) since the length of the gel/water interface decreases with increasing water flow rate. The penetration depth of the gel/water interface decreases with increasing water flow rate. For water velocity of the order of a metre per year the gel may penetrate several metres into the fracture when steady state is reached.

The simulations were made with only sodium as counterion. Most simulations had sodium concentrations below the critical coagulation concentration, CCC. In the compacted bentonite at the fracture mouth it was 10 mM and 0.1 mM in the approaching water. At these concentrations the gel is expansive and can turn into a sol releasing colloidal particles. The low ion concentration has a strong impact on the fluid viscosity, which increases with decreasing ionic strength. At the same time, however the repulsion forces between the smectite particles increase causing a quicker expansion. Simulations with higher sodium concentrations had a marginal influence on the erosion rate.

For the highest water flow rates the smectite loss could be up to 0.3 kg per year for one canister. This is more than one order of magnitude larger than what could be reached by smectite particle diffusion alone if fluid flow was neglected.

In experiments in downward facing slits (fractures) it has been found that bentonite releases gel agglomerates much faster than expected. These are released and sediment also under conditions where it is expected that the smectite particles should have separated into individual smectite sheets, which would not noticeably be influenced by gravity. The reasons for this behaviour are not understood.

In the modelling it is assumed that there are no other larger non-smectite particles that would be left behind to gradually build up a bed of particles that could act as filter, slowing down or even straining further smectite penetration into the fracture. The modelling results could therefore be highly pessimistic because bentonites contain tens of percent of accessory minerals that do not form colloids and the presence of which may cause the expansion to be slowed down by friction against the fracture walls. An overview of mechanisms and models for bentonite erosion may be found in Neretnieks et al. (2009).

Contents

1 Introduction

Several countries plan to use bentonite clay as buffer and backfill material in nuclear waste repositories. Bentonite, which contains montmorillonite, a smectite mineral, swells strongly in contact with water. Compacted bentonite around the canister protects it from chemical and mechanical disturbances. Should large amounts of bentonite be lost by erosion the canister would be less protected. It might corrode faster and release of nuclides would also increase if the canister is breached. We will use the term smectite for the clay particles and fluid or gel/sol for the expanding clay.

Bentonite consists mostly of tiny smectite clay particles. The particles are very thin compared to the other dimensions. In addition the bentonite may contain tens of percent of accessory minerals such as quartz, feldspar, calcite, gypsum etc. The smectite particles are negatively charged on their faces and the charges are compensated by cations that reside in a thin diffuse layer associated with the particles. When the smectite particles are at close distances they strongly repel each other. This causes the strong swelling pressure in compacted wet bentonite. In dilute waters dominated by monovalent ions such as sodium the repulsion between the smectite particles can overcome any attractive forces between them and expand to form dilute stable suspensions that behave essentially as water. The suspension can flow if subject to a hydraulic gradient. In this report, we neglect any influence of accessory minerals that may be left behind forming a porous bed with pores through which the smaller smectite particle have to migrate.

In this report we consider a very wide range of volume fraction of smectite in the clay ranging from 40% in the compacted buffer at the mouth of the fracture, decreasing over tens of percents to some percents in the expanded bentonite gel in the fracture and down to fractions of percents in the very dilute suspension we call sol. We make no distinction between compacted bentonite and the more dispersed one in our model and call it gel. In the dilute sol the particles can move independently of each other. For illustrative purposes we use the term gel/water interface although there is a gradual change from gel to sol.

The swelling pressure is influenced by the ionic strength of the pore water, which is influenced by the composition of the water seeping in the rock. In high ionic strength waters the clay gel is stable once it has expanded to a density when attractive and repulsive forces between smectite particles balance. At this point the gel is cohesive and will not either expand or contract. Under such conditions very little or no smectite can be released into the seeping water in the fracture. However, at low ionic strengths repulsive forces dominate over attractive forces at all gel densities. The gel is repulsive and the smectite particles can be released as colloids and form stable sols, which may be carried away by the flowing water.

The critical coagulation concentration, CCC, of counterions is the concentration in the pore water above which the gel is cohesive. The CCC is much higher for monovalent cations than for divalent cations. The term CCC is often loosely used to denote the concentration of monovalent or divalent ions in the pore water. It is not defined for mixtures of differently charged ions in the pore water. It is likely that in addition to the ionic strength that influences the thickness of the diffuse layer also the composition of ions within the electrical diffuse layer plays an important role. Because of the strong preference for divalent ions in the diffuse layer the composition there and in the “free” water can be very different. Birgersson et al. (2009) and Jönsson et al. (2009) discuss these effects and their causes. Neretnieks et al. (2010b) discuss how the pore water composition at the gel/water interfaces is influenced by the combined effects of ion exchange in the clay and ion transport between the gel and the seeping water for competing mono- and divalent ions. In this communication we only account for the presence of a migrating monovalent cation, sodium. There are several reasons for this. Sodium clays are considerably more studied and more data are available. Calcium dominated clays form larger particles that are less mobile by Brownian forces. Calcium dominated clays do not swell as much and do not release sol particles as readily as sodium dominated clays. Practically no information is available for the rheological properties of calcium-dominated clays at lower volume fractions.

Should the conditions favour a cohesive gel to develop, erosion by colloid generation will not take place. Erosion by flow under such conditions might take place if the gel viscosity is low enough but we have not been able to obtain reliable rheological data on cohesive gels that could be used for such modelling.

Bentonite intrusion into a fracture is a complex process where several different and sometimes competing mechanisms are active simultaneously. When the bentonite in the deposition hole is in contact with dilute water the bentonite expands and intrudes into the fracture moving further and further into the fracture. The rate of expansion and intrusion is determined by the balance of different forces acting on the particles. We consider the gravitational and buoyancy forces, the viscous drag force, the diffusional driving force (giving rise to Brownian motion), the van der Waals attractive force, and the repulsive forces caused by the diffuse double layer repulsion (Liu et al. 2009a). The gel becomes increasingly less dense the further out in the fracture it has expanded. The viscosity of the gel/ sol fluid increasingly approaches that of water and the gel can flow. In addition, at the gel/ water interface, particles are released as colloids into the seeping water in the fracture. A steady state is reached where bentonite ingresses into the fracture with the same rate as it is released into the seeping water.

The flow of the fluid (gel/sol/water) in the fracture is modelled by the Darcy equation where the gel/ sol/water is considered as a fluid with viscosity varying with gel density and ion concentration in the pore water. The viscosity of the fluid increases rapidly with increasing bentonite volume fraction. For high smectite volume fractions, the viscosity is many orders of magnitude larger than that for the water and it becomes increasingly non-Newtonian and acquires thixotropic properties that are not readily modelled.

The viscosity is also strongly influenced by the ion concentration because the electrical double layer extends farther from the particles at low ionic strengths and the particles interfere with each other even at low solid volume fractions. We have developed a simple model for the viscous behaviour of the gel/sol for an expansive gel based on experimental data from the literature useful for dilute gel/sols.

The overall model we use includes a sub-model for smectite expansion and colloid release, a model for flow of the gel/sol and a model for flow and diffusion of a monovalent cation and its accompanying anion. The setting is that there is a compacted strongly swelling bentonite in a deposition hole intersected by a fracture where dilute water seeps. The water ingresses and dilutes the gel forming a fluid that can flow. The gel can also release colloid particles forming a sol that flow essentially as water. Flow of gel and sol combine to erode the smectite. The fracture is modelled as a constant aperture fracture with a certain transmissivity and the flow of the fluid is driven by a hydraulic gradient.

A number of short appendices give details on some of the issues discussed in the report.

2 Governing equations

The expansion of the bentonite, the diffusion of the cation and the fluid flow takes place in two dimensions and therefore a two-dimensional model is used. The modelling comprises the following mechanisms and models:

- The gel/sol/water fluid flow in the fracture is described by the Darcy equation.
- The expansion of bentonite into the fracture is described by a dynamic force balance model for colloidal expansion developed by Liu et al. (2009a).
- The transport of the ions in the bentonite pore water includes advection and diffusion.
- The viscosity relation is simplified but based on experimental data for dilute, expansive gels.

The viscosity of the fluid is a function of the smectite volume fraction and the concentration of the counterion, sodium in this case. The diffusion coefficient for the cation is also a function of the smectite volume fraction. All equations are strongly coupled and are solved simultaneously.

2.1 Darcy equation

We model the flow of the fluid consisting of a gel/sol and water with the Darcy equation. The viscosity of the gel is very strongly dependent on the volume fraction of smectite in it. Where the viscosity is large the gel will flow very slowly. Where the viscosity is lower the gel flows more rapidly. Inside the gel there is a relative movement between particles and water in the expanding gel. The friction between water and the particles is important, as it determines the rate at which the gel expands taking up water. This is discussed in the Section 2.3.

The Darcy equation is slightly modified to account for varying viscosity of the fluid. The transmissivity T of a fracture depends on the viscosity of the fluid. Rock fracture transmissivities are usually given for water and can directly be obtained for another fluid viscosity by

$$T = T_w \frac{\eta_w}{\eta} \tag{2-1}$$

The subscript w stands for water. T (m^2/s) is the fracture transmissivity and η ($N\ s/m^2$) the viscosity of the fluid. The Darcy equation is used to calculate the fluid velocity field, which however is strongly coupled to sodium and smectite concentration.

$$\vec{u} = \frac{T \cdot \vec{i}}{\delta} \tag{2-2}$$

where $\vec{u}$ (m/s) is the fluid velocity and $\vec{i}$ (m/m) the hydraulic gradient vectors. δ is the fracture aperture (m).

2.2 The Diffusion equation for sodium

The advection-diffusion equation is used to model sodium migration in the fluid. Only the cation needs to be modelled as the anion transport is obtained from the charge balance. Sodium is used as the migrating cation as this is the dominating species in the systems considered. The advection-diffusion equation is given by

$$\frac{\partial c}{\partial t} = -\vec{u}\nabla c + \nabla \cdot \left(D \nabla c\right) \tag{2-3}$$

where c (mol/m^3) is the concentration of the cation, D (m^2/s) the diffusion coefficient and t (s) is time. An isotropic system is assumed, therefore D is a scalar but it varies with gel density. The left hand side term is the accumulation term. The first term on the right hand side denotes the advective transport and the second the diffusive transport.

2.3 Smectite expansion equation

The smectite expansion model is described in Liu et al. (2009a). It is summarized here. The equation describing the mass balance for smectite in the system is similar to the advection-diffusion equation and is given as

$$\frac{\partial \phi}{\partial t} = \vec{F}_s \nabla\left(\frac{\phi}{f}\right) - \vec{u}\,\nabla\phi + \nabla\cdot\left(\frac{\chi}{f}\nabla\phi\right) \tag{2-4}$$

where F_s (N) accounts for the gravitational force and the buoyant force, ϕ the volume fraction of smectite in the fluid and χ (J) the sum of the energy of the particles. This term comprises the energy from the thermal motion and the energy due to the van der Waals and electrostatic forces. The ratio χ to f can be considered as a diffusivity, where $f = f_{fr}/(1-\phi)$ considers that smectite is moving into the fracture and an equivalent volume of water is moving in the opposite direction. f_{fr} (N s/m) is the friction coefficient between particles and water. It is given by

$$f_{fr} = 6\pi\eta_w r_{eq} + V_p k_0 \tau^2 a_p^2 \eta_w \frac{\phi}{(1-\phi)^2} \tag{2-5}$$

where r_{eq} (m) is the equivalent radius of the non-spherical particles. It can be obtained for arbitrarily shaped particles. k_o is the pore shape factor, τ the tortuosity of the flow channels in the gel (the product $k_o\tau^2$ is often called Kozeny's constant). V_p(m^3) denotes the volume of the particles and a_p (m^2/m^3) the specific surface area per unit volume of particles. The equation combines the friction for a single particle in very dilute sol with that of a particle in porous gel bed (Liu et al. 2009a). In this application we have used the Kozeny-Carman expression although it has been found that it must be modified somewhat depending on the type of clay and composition of water (Liu 2010).

The function χ is given by

$$\chi = k_B T + (h+\delta_p)^2\left(\frac{\partial F_A}{\partial h} - \frac{\partial F_R}{\partial h}\right) \tag{2-6}$$

where k_B (J/K) is the Boltzmann constant, T (K) denotes the absolute temperature, h (m) is the separation between the flat particles and δ_p (m) is the particle thickness, F_A*(N) and* F_R*(N)* denote the van der Waals attractive forces and electrical repulsive forces respectively. Explicitly, the partial derivative of the van der Waals force with respect to the separation can be given by

$$\frac{\partial F_A}{\partial h} = -\frac{A_H S_p}{2\pi}\left[\frac{1}{h^4} - \frac{2}{(h+\delta_p)^4} + \frac{1}{(h+2\delta_p)^4}\right] \tag{2-7}$$

where A_H (J) is the Hamaker constant and S_p (m^2) the particle surface area. The partial derivative of the electrostatic double-layer force with respect to the separation can be written as (Liu and Neretnieks 2008),

$$\frac{\partial F_R}{\partial h} = -4\kappa c RTS_p \tanh y^m\left[\cosh y_\infty^m \sinh\left(\frac{y_\infty^m}{2}\right) + \frac{1}{\kappa h}\sinh y_\infty^h + \frac{2}{(\kappa h)^2}\sinh\left(\frac{y_\infty^h}{2}\right)\right] \tag{2-8}$$

with

$$y^m = \sinh^{-1}\left[2\sinh y_\infty^m + \frac{4}{\kappa h}\sinh\left(\frac{y_\infty^h}{2}\right)\right] \tag{2-9}$$

$$y_\infty^m = 4\tanh^{-1}\left[\tanh\left(\frac{y_\infty^0}{4}\right)\exp(-\kappa h/2)\right] \tag{2-10}$$

$$y_\infty^h = 4\tanh^{-1}\left[\tanh\left(\frac{y_\infty^0}{4}\right)\exp(-\kappa h)\right] \tag{2-11}$$

κ is the reciprocal Debye length (m^{-1}), which is

$$\kappa = \left(\frac{2F^2 c z^2}{\varepsilon_0 \varepsilon_r RT} \right)^{1/2} \tag{2-12}$$

F (C/mol) is the Faraday constant, z is the valence, ε_o (F/m or C/V/m) denotes the permittivity in vacuum, ε_r is the relative permittivity. The term y is the dimensionless potential defined as

$$y = \frac{zF\psi}{RT} \tag{2-13}$$

where ψ (J/C) is the electrical potential and y_∞^0 is the surface potential of an isolated plate

$$y_\infty^0 = 2\sinh^{-1}\left(\frac{s^0}{2} \right) \tag{2-14}$$

with a dimensionless surface charge density, s^0, given by

$$s^0 = \frac{zF\sigma^0}{\varepsilon_0 \varepsilon_r \kappa RT} \tag{2-15}$$

σ^0(C/m^2) is the specific charge on the particle surface.

In these calculations the gravity force was found to be negligible so Equation (2-4) reduces to

$$\frac{\partial \phi}{\partial t} = -\bar{u}\nabla\phi + \nabla \cdot \left(\frac{\chi}{f} \nabla \phi \right) \tag{2-16}$$

2.4 Correlations used

The Sodium diffusion coefficient in the fracture is assumed to be reduced by the presence of the smectite particles. Tests with different relationships have shown that for the present application the results are not very sensitive to the diffusion coefficient. For this reason, the relationship used for the diffusion is somewhat arbitrarily given by

$$\frac{D}{D_o} = (1-\phi)^{1.6} \tag{2-17}$$

The value of D_o is taken to be $2 \cdot 10^{-9}$ m^2/s.

The viscosity of the gel/sol is a function of the smectite volume fraction and the cation concentration in the water. We use a relationship developed using the co-volume concept which is shortly described below.

For a dilute suspension of uncharged spherical particles the relative viscosity is given by the Einstein equation (Bird et al. 2002)

$$\frac{\eta}{\eta_o} = 1 + 2.5\phi \tag{2-18}$$

The coin-like smectite particles rotate due to Brownian motion and need a co-volume equal to a sphere in which the coin can rotate freely. If in addition, the particle is charged and the thickness of the diffuse layer is added to the diameter of the coin the co-volume becomes even larger. We tested the idea that such a co-volume could be used instead of the volume of a rigid sphere in the Einstein equation. In addition, higher order terms were added to extend the range of the equation to not only very dilute suspensions. More background to the notion of co-volume can be found in Neretnieks et al. (2009). Fitting a number of experimental data (Adachi et al. 1998) gave the following results:

$$\frac{\eta}{\eta_o} = 1 + 1.022\phi_{cov} + 1.358\phi_{cov}^3 \tag{2-19}$$

The data upon which the results are based range over $0.0003 < \phi < 0.009$ and sodium concentration between 0.6 and 10 mM. The measured relative viscosity ranges from 1 to 5.5. The co-volume fraction ranges from 0 to 130%. The range of volume fraction in these experiments is much less than what we use in our modelling but the equation ensures that the viscosity increases very rapidly with increasing smectite content.

The co-volume fraction is defined as

$$\phi_{\text{cov}} = \frac{2}{3}\frac{\left(D_p + 2m\kappa^{-1}\right)^3}{D_p^2\delta_p}\phi \qquad (2\text{-}20)$$

with the Debye length k^{-1} given by,

$$\kappa^{-1} = \sqrt{\frac{\varepsilon_0 \varepsilon RT}{2IF^2}} \qquad (2\text{-}21)$$

where I is the ion strength. A value of m=1 is used for m in Equation 2-20. Figure 2-1 shows the relative viscosity η/η_w as a function of the smectite volume fraction and the sodium concentration for four different sodium concentrations. It is seen that low sodium concentrations will strongly increase the viscosity of the fluid.

Rheological data have been obtained for sodium-exchanged bentonites over a wide range of smectite volume fractions (Birgersson et al. 2009). They show that the gels become increasingly more viscous and much more non-Newtonian at volume fractions above the percent level. Thixotropic effects also become increasingly more important at smectite volume fractions larger than about 1%. The use of a Newtonian viscosity model becomes increasingly wrong but we have found no viable alternative. We have chosen to extrapolate Equation (2-19) over the full range used in the simulations. This is defensible because the simulation results show that the gel will be so viscous at higher volume fractions that it will contribute very little to the transport of smectite due to gel flow.

It is seen in Figure 2-1 that the viscosity approaches that of water at volume fractions less than about 0.5%. Water with a higher concentration would flow slower in proportion to the relative viscosity for the same hydraulic gradient. So for example a dilute suspension remaining in a part of an eroded deposition hole would practically flow as water at lower concentrations but would be to viscous to flow much for volume fractions above a few %.

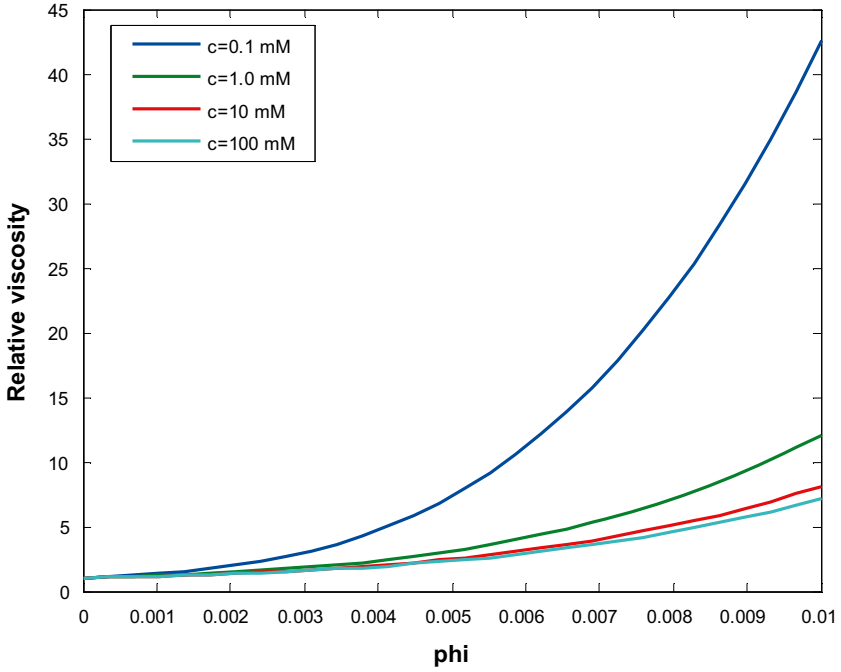

Figure 2-1. *Relative viscosity as function of the smectite volume fraction ϕ for different sodium concentrations.*

3 Calculated Cases

3.1 Simplified geometry

The intersection between the deposition hole and the fracture is taken to be a straight line in the simplified model. The fracture is 1 m long in the flow direction with a depth sufficient to act as boundary at infinite distance. Different depths are used for different flow velocities to economise on computer time. For small velocities the gel penetration into the fracture is expected to be very large, therefore a larger depth is used. The distance to the outer boundary will have a marginal effect on the results. The water flow is from the left to the right and the fracture aperture is 1 mm.

The boundary conditions are shown in Figure 3-1. At the fracture mouth, lower boundary in the figure, the volume fractions of smectite and sodium concentration are held constant. This implies that bentonite and sodium will enter the fracture over this boundary. At the left hand boundary a constant hydraulic head is assigned allowing water with its sodium to flow in but there is no flux of smectite over this boundary. At the right hand boundary constant head is imposed. This allows convective flow of the fluid with its smectite, water and sodium to leave. The top boundary is closed.

The depth of the fracture in the direction perpendicular to the regional flow is different for different fracture transmissivities. For the larger water flow rate, 315 m/yr (fracture aperture of 10^{-3} m, fracture transmissivity of $1.0 \cdot 10^{-7}$ m^2/s and a hydraulic gradient of 0.1) the depth of the fracture was 1 m. For the lower flow rate, 3.15 m/yr (fracture transmissivity of $1.0 \cdot 10^{-9}$ m^2/s) the fracture depth was about 6.0 m.

The smectite volume fraction ϕ at the fracture mouth is 0.40. The sodium concentration in the porewater at this boundary is 10 mM. It is 0.1 mM in the approaching seeping water in the first set of calculations. The concentrations are varied in later simulations to test the impact of the sodium concentration.

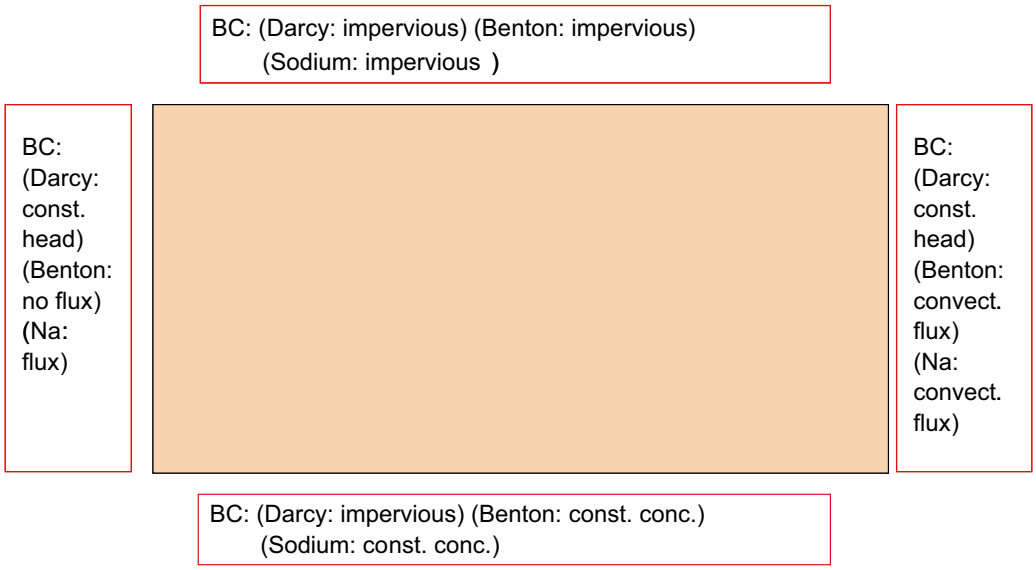

Figure 3-1. *Boundary conditions for simplified geometry.*

3.2 Cylindrical symmetry

Most of the simulations were made with the simplified geometry since its computation was faster and numerically more stable. Based on the experiences from these simulations a more realistic case was built with flow around a circular deposition hole, which is shown in Figure 3-2. The boundary conditions are similar to those used in the base case. At the fracture mouth, the smectite volume fraction of 0.40 keeps constant over time. Constant concentration is also assumed for the sodium at the fracture mouth as well as in the approaching water. At the border opposite to the canister deposition hole, impervious boundary conditions are used. At the vertical borders, constant heads are used creating a water flow from left to the right. No smectite or sodium can leave over left border but upstream migration of smectite as well as of sodium is allowed. The fluid with smectite and sodium leaves through the right boundary. An important difference between the simplified and the cylindrical case is that in the latter, smectite as well as sodium are also allowed to migrate upstream. In addition, the length of the gel/water interface will increase with penetration depth.

In most cases sodium concentrations below the CCC were used. Typically 10 mM at the internal border and 0.1 mM for the concentration of the seeping water. The regional hydraulic gradient is 0.1 in all calculations and the fracture aperture is 1 mm.

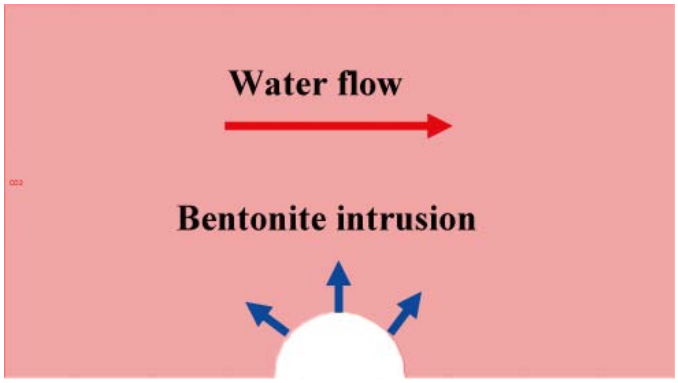

Figure 3-2. *Modelled fracture including the fracture around the canister deposition hole.*

4 Results for the rectangular geometry

Figure 4-1 shows the smectite volume fraction distribution in the fracture and the fluid velocity for a undisturbed water velocity of 315 m/yr. The fluid flow is only important in the zone where the smectite volume fraction is below about 1–2%. The fluid velocity decreases rapidly when the smectite volume fraction approaches a few percent. Figure 4-2 shows the sodium concentration distribution for the same situation.

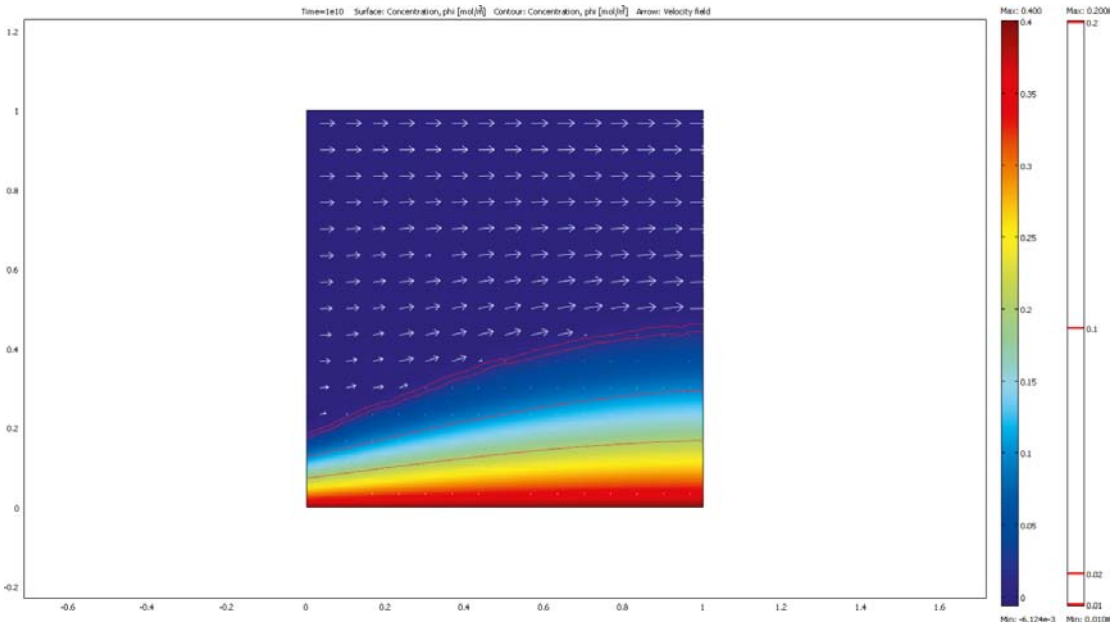

Figure 4-1. *Smectite volume fraction distribution and water velocity field in the fracture. The contour lines show the smectite volume fraction at levels of 0.01, 0.05, 0.10, and 0.20, from top down.*

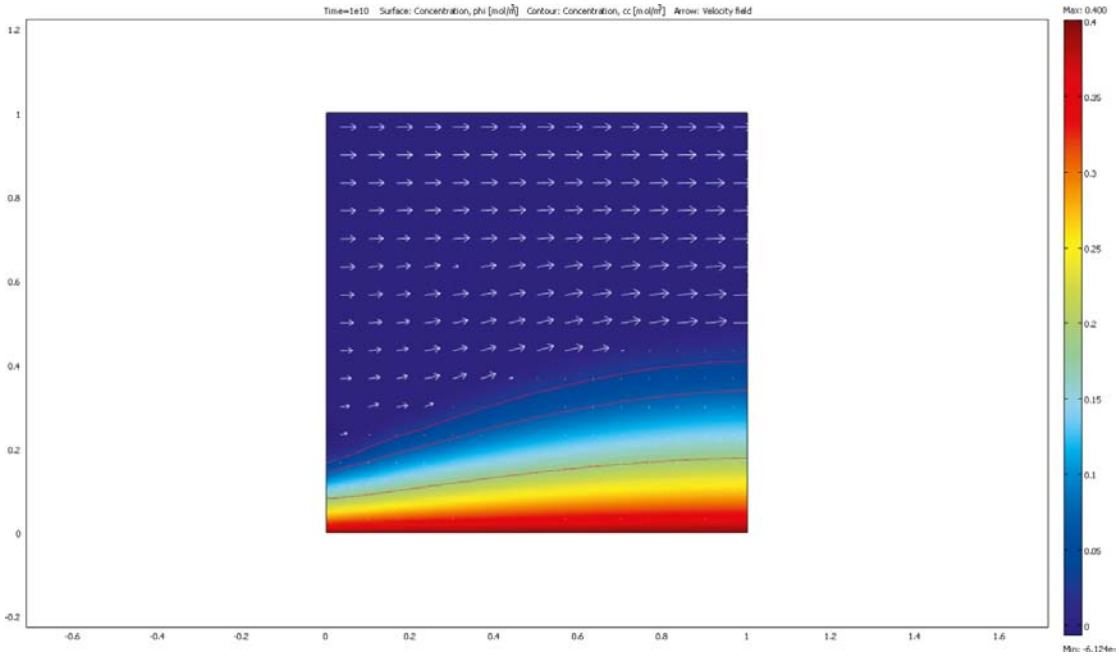

Figure 4-2. *Sodium concentration distribution and water velocity field in the fracture. The contour lines show the sodium concentration at levels of 1, 2, and 5 mM, from top down.*

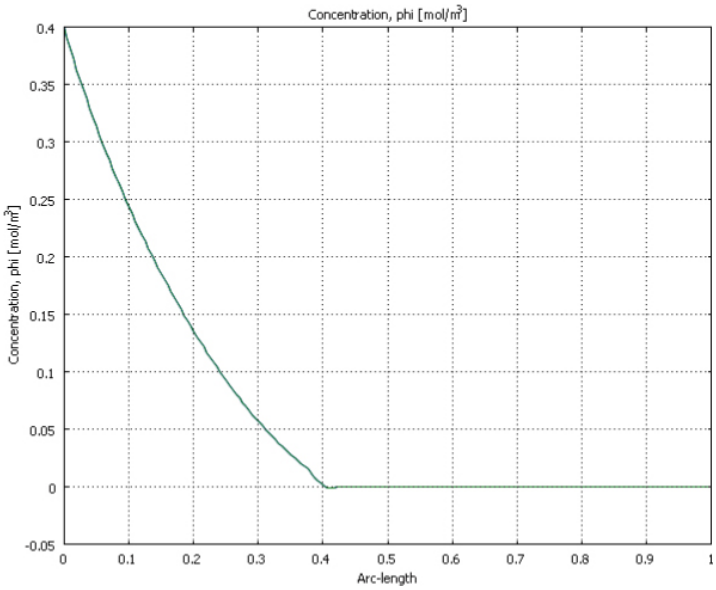

Figure 4-3. *Smectite volume fraction profile at the fracture centre from the bottom to the top. On the horizontal axis, the value 0.0 m is at the fracture mouth and 1.0 m is at the upper boundary.*

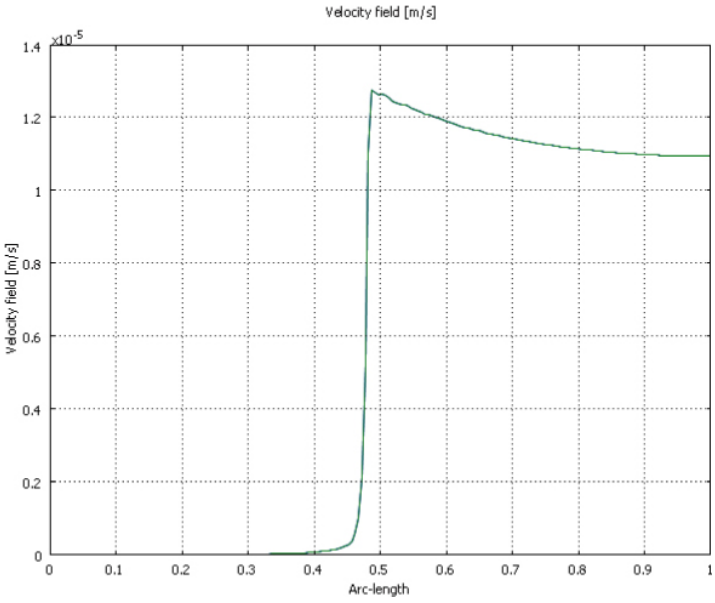

Figure 4-4. *Fluid velocity at right hand side boundary. On the horizontal axis, the value 0.0 m is at the fracture mouth and 1.0 m is at the upper boundary.*

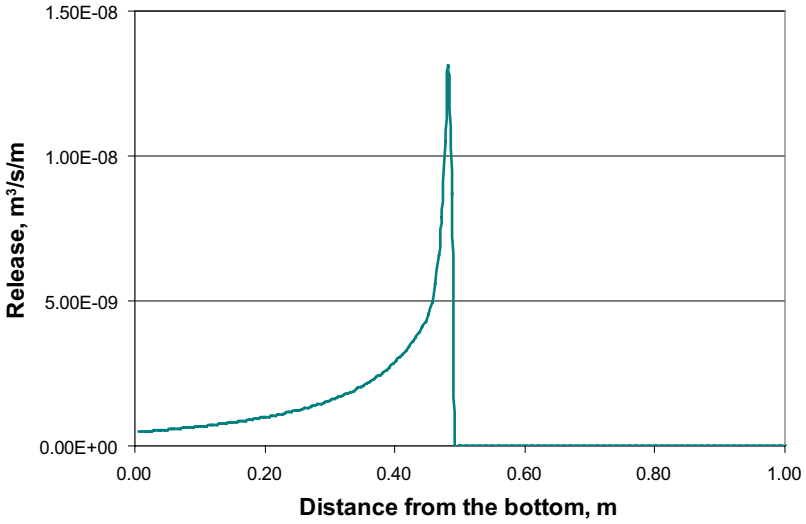

Figure 4-5. *Smectite release rate through the right hand side boundary.*

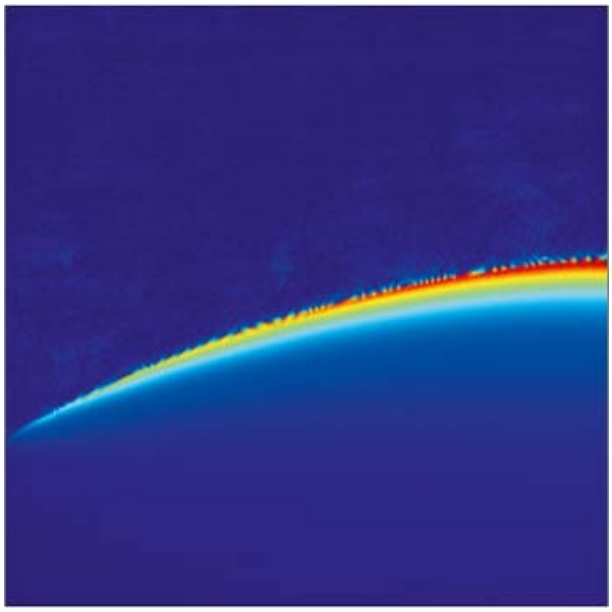

Figure 4-6. *Release of bentonite along the gel/water interface. The size of the fracture is 1 m wide and 1 m high.*

Figure 4-3 shows the smectite volume fraction profile along a vertical line at 0.5 m from the left boundary, extending from the bottom to top. On the horizontal axis, the value 0.0 m is at the fracture mouth. 1.0 m is at the top boundary. The figure shows that the smectite volume fraction is negligible for distances larger than 0.4 m. This justifies the no-flux condition used for the smectite through the top boundary. All the smectite introduced into the fracture through the fracture mouth escapes through the right hand border. Integrating the smectite fluxes through these boundaries give the same results supporting the accuracy of the numerical solution.

The fluid velocity and smectite release rate at the right hand side boundary are shown in Figures 4-4 and 4-5. The smectite release rate is calculated by the product of water velocity and smectite volume fraction neglecting particle diffusion.

The release of bentonite takes place mostly in locations close to the gel/sol interface. Figure 4-6 shows the flux of bentonite along this interface the release of bentonite along this interface. The figure presents the product of water velocity times bentonite volume fraction. It is seen that the transport is concentrated to a very narrow region.

4.1 Effect of the water flow rate

Simulations were carried out for different water velocities, corresponding to different fracture transmissivities. These were varied from $1.0 \cdot 10^{-9}$ m^2/s to $1.0 \cdot 10^{-7}$ m^2/s. For a fracture with an aperture of 1.0 mm and a hydraulic gradient of 0.1 the undisturbed water velocity varies from 3.15 m/yr to 315 m/yr. The smectite loss was calculated for these water velocities. In addition the location of the gel/water interface (location where the smectite volume fraction is below 0.01%), i.e. the penetration depth was determined at the right hand boundary. The results are shown in Table 4-1 and Figure 4-7 and 4-8.

From the figures it is seen that smectite release increases with the square root of the water velocity. At the same time the distance to the smectite border decreases with the square root of the water velocity.

Table 4-1. Smectite release for a fracture of 1 mm aperture and distance to the gel/water interface for different water velocities.

Water velocity, m/yr	Smectite release, kg/yr/m	Penetration depth at the right hand boundary, m
3.15	0.006	4.3
9.45	0.011	2.5
31.5	0.022	1.3
94.5	0.039	0.8
315	0.072	0.5

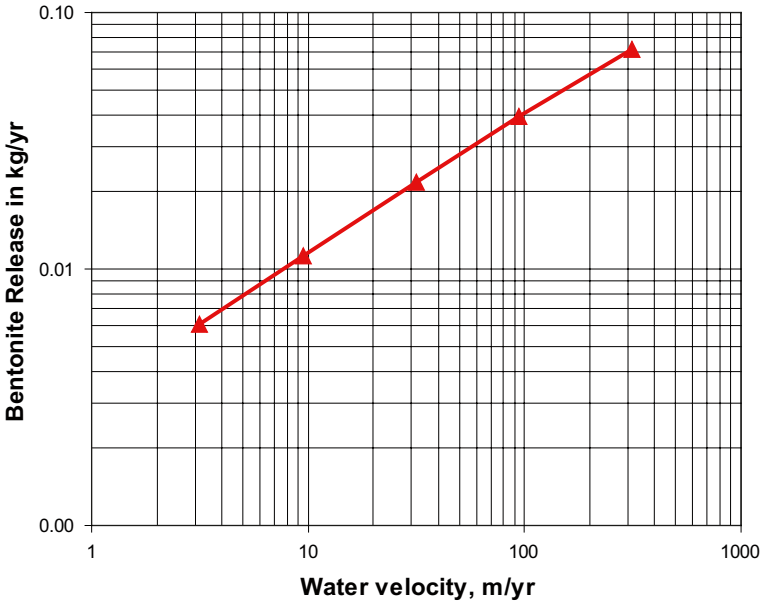

Figure 4-7. *Smectite release (kg/yr) in a one metre fracture with an aperture of 1 mm for different water velocities.*

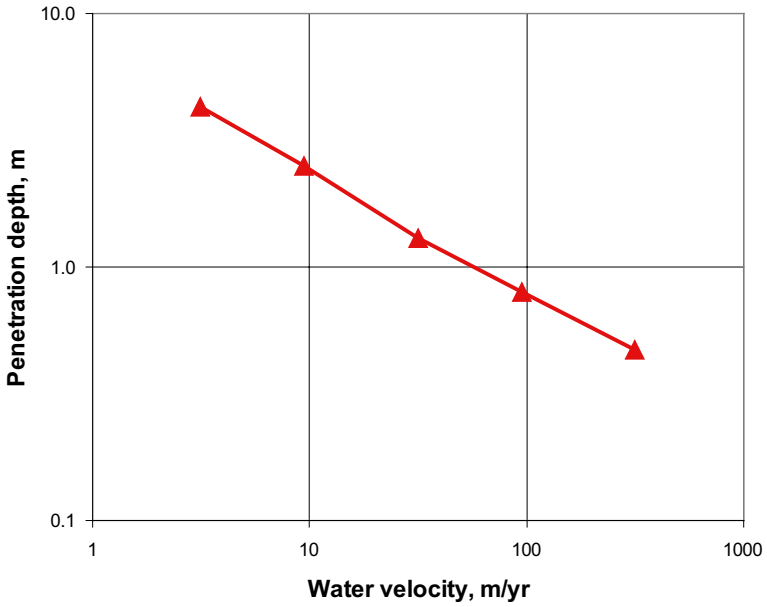

Figure 4-8. *Distance to the gel/water interface for different water velocities.*

5 Results for cylindrical symmetry

The fracture size in this case is at least 10 m times 5 m with a cylindrical deposition hole 1.75 m in diameter. Larger fracture sizes were used for lower water velocities. The pattern of the results is similar to those for the rectangular geometry. The numerical calculations using the cylindrical geometry are somewhat unstable due, possibly, to the existence of a stagnation point in the velocity field. In order to obtain a more stable solution, artificial diffusion along streamlines was used in the numerical scheme. Since artificial diffusion may add dispersion to the real solution, the factor that controls the amount of artificial diffusion is chosen as small as possible. In our calculations the streamline upwind Petrov-Galerkin artificial diffusion with a factor of 0.03 was used.

The smectite volume fraction and the velocity field are shown in Figure 5-1 for the large water velocity 315 m/yr. Figure 5-2 shows the same results for a fracture with a ten times smaller water velocity.

It is seen in the figures that the smectite migrates upstream in this case. As in the rectangular case the gel/water interface moves further into the fracture with lower water velocities.

5.1 Effect of the water flow rate

The seeping water velocity was varied from 0.10 to 315 m/yr. The smectite release was calculated for a fracture aperture of 1.0 mm and the results are shown in Table 5-1. The smectite release as a function of water flowrate is shown in Figure 5-3 and the location of the interface gel/water interface is shown in Figure 5-4. The smectite release and the penetration depth into the fracture for the two lowest water velocities (0.1 and 0.32 m/yr) were determined by extrapolation from data for the larger velocities.

The release of smectite into the seeping water increases with the water velocity with an exponent about 0.4. For the rectangular geometry the exponent was 0.5. The smaller exponent is due to that when the water velocity decreases the length of the gel/water interface increases facilitating the smectite particle migration.

From Figure 5-3, the erosion rate $R_{Erosion}$, in the fracture in kg/yr can be expressed as,

$$R_{Erosion} = A \cdot \delta \cdot v^{0.41} \qquad (5\text{-}1)$$

where v is the water velocity in m/yr, δ the fracture aperture in m, and the constant A takes the value 27.2

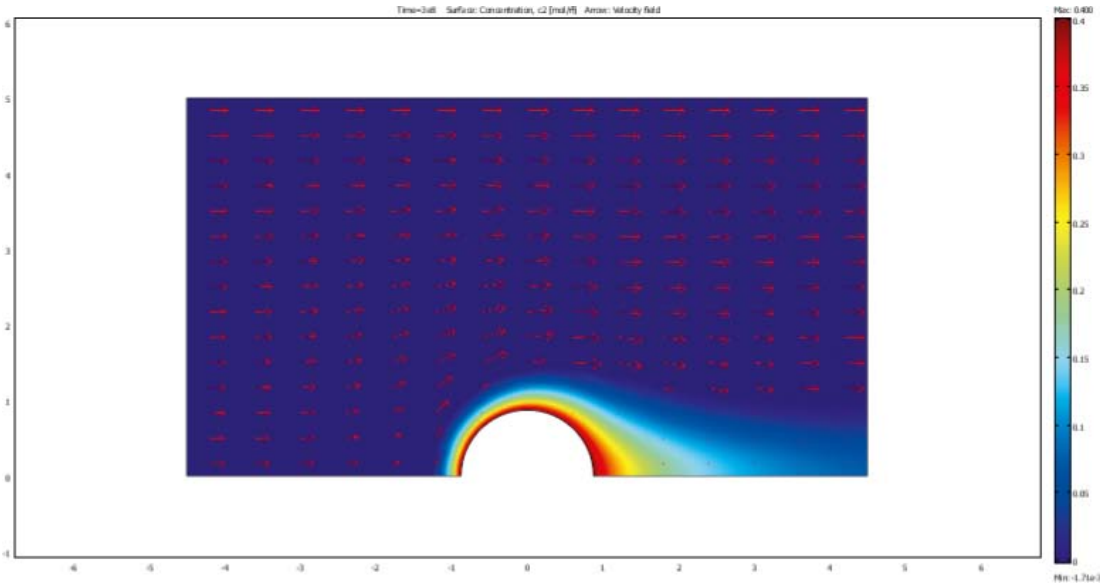

Figure 5-1. *Smectite volume fraction distribution and velocity field (as arrows) for an approaching water velocity in the fracture of 315 m/yr.*

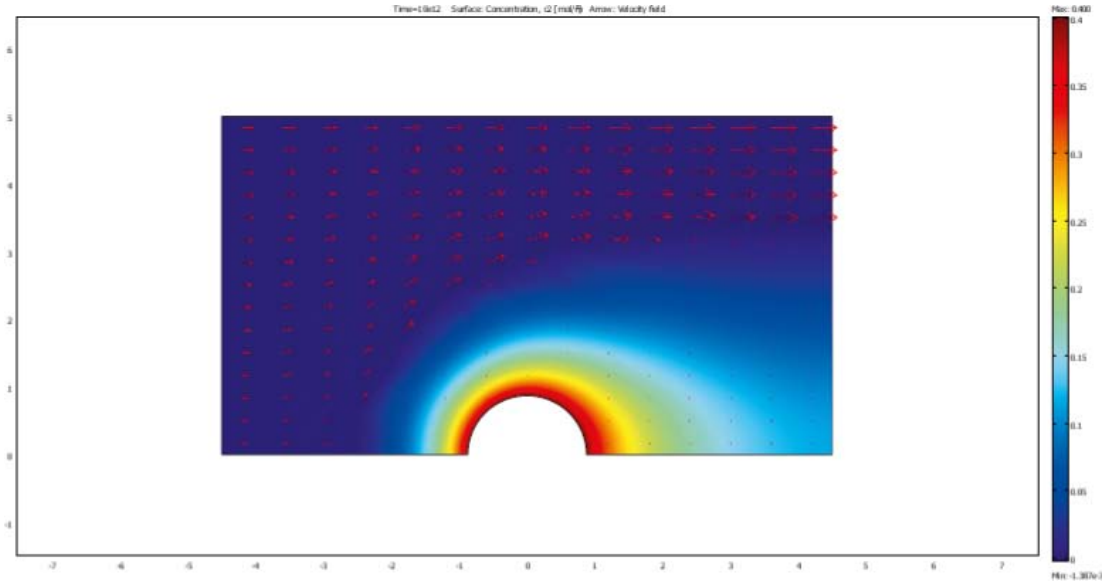

Figure 5-2. Smectite volume fraction distribution and velocity field (as arrows) for a water velocity of 31.5 m/yr.

Table 5-1. Results for cylindrical symmetry, for different transmissivities, a hydraulic gradient of 0.1 and fracture aperture 1 mm.

Water velocity, m/yr	Smectite release, kg/yr	Distance to gel/water interface m
0.10	0.011	34.6
0.32	0.016	18.5
0.95	0.026	11.5
3.15	0.043	7.0
9.45	0.071	4.1
31.50	0.117	2.1
94.50	0.180	1.0
315.00	0.292	0.5

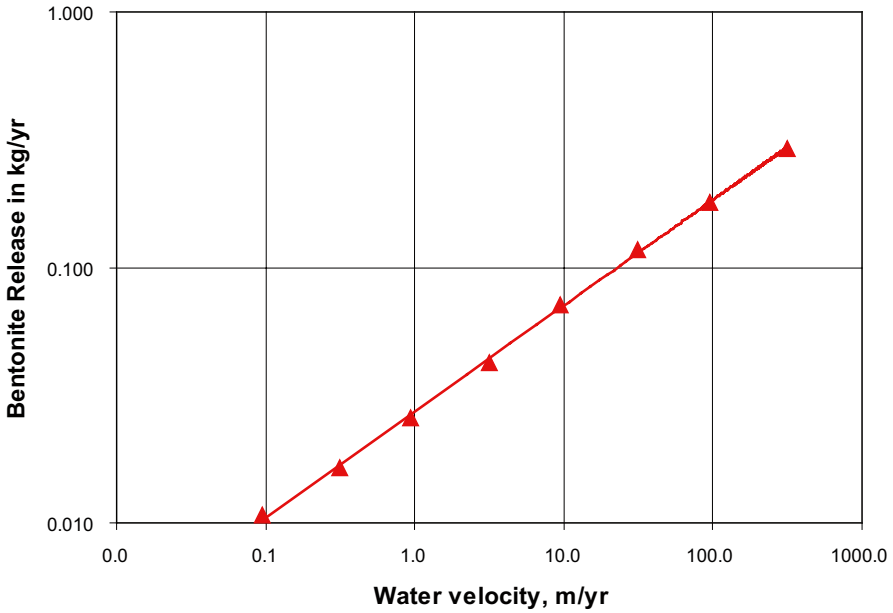

Figure 5-3. Smectite release for different fracture transmissivities.

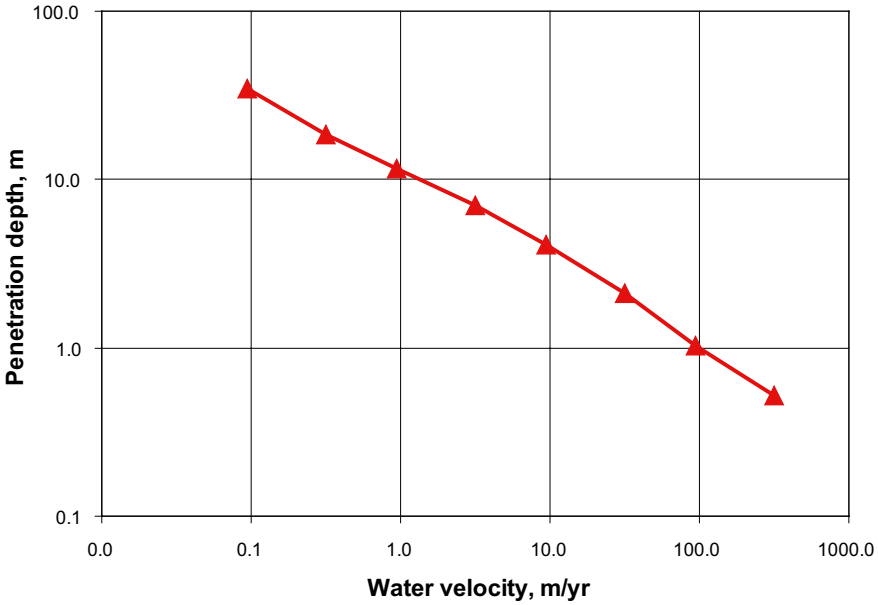

Figure 5-4. *Penetration depth of gel/water interface into the fracture for different fracture transmissivities.*

5.2 Discussion of the results

5.2.1 Influence of sodium concentration

In the calculations presented above the sodium concentration is below the CCC everywhere. In this section we present some simulations where at least near the fracture mouth the sodium concentration is above the CCC. Our smectite expansion model actually includes effects of concentrations of monovalent ions above the CCC because it accounts for the attractive van der Waals forces as well as the repulsive double layer forces. The latter will decrease with increasing ion concentration and can be overwhelmed by the attractive forces not permitting the gel to expand further than the volume fraction at which this occurs (Liu et al. 2009b).

In our model we account for the diffusion of sodium from the deposition hole towards the seeping water and it becomes a question whether the sodium can move rapidly enough to supply the pore-water at the gel/water interface with a concentration above the CCC before the sodium is lost to the seeping water. Should the concentration of sodium at that boundary be at or above the CCC no smectite could be lost by smectite particle diffusion. More importantly, the gel becomes cohesive and more viscous. It does not flow as readily at the volume fraction of smectite expected at the gel/water boundary. For sodium as counterion the volume fraction at which this occurs is on the order of some percent. The viscosity of the gel can then be expected to be considerably larger than that of water (Liu et al. 2009b). However, we have not been able to find reliable experimental viscosity data to model this.

The smectite expansion in the fracture could be expected to be lower for concentrations above the CCC and a lower release of smectite into the seeping water may be expected. However, the smectite release could be increased, to some extent, due to the larger concentration of the counterion (sodium) in the zone close to the gel/water interface and the resulting lower viscosity.

Some simulations were made to study the effect of higher sodium concentrations in the compacted bentonite allowing a larger rate of supply of sodium. The rectangular geometry was used with a water velocity of 94.5 m/yr. In one simulation a value of 100 mM for the sodium concentration at the fracture mouth was used, while the sodium concentration of the seeping water was 1.0 mM. The CCC for sodium is about 50 mM. In another simulation, the sodium concentration of the seeping water in the fracture was increased to 10.0 mM.

When the sodium concentration in the smectite porewater is 100 mM and the seeping water concentration is 1.0 mM, the smectite release is decreased by about 10%; from 0.039 kg/yr/m to a value of 0.035 kg/yr/m. Figure 5-5 shows the smectite profile. At these sodium concentrations the smectite profile is sharper at the smectite/water interface. The sodium concentration at the gel/water interface was 3.5 mM, which is clearly below the CCC.

In another simulation the sodium concentration in the water was increased to 10 mM, maintaining the smectite pore water concentration in 100 mM. Also in this case the sodium concentration at the gel/water interface was below the CCC, 12.5 mM. The smectite release decreases to a value of 0.033 kg/yr/m.

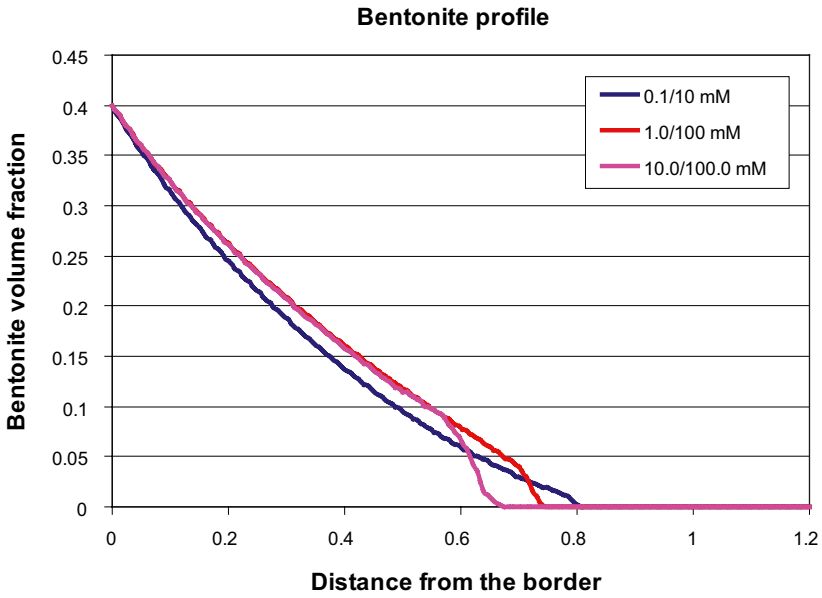

Figure 5-5. *Smectite volume fraction profiles for different sodium concentrations in the pore water.*

6 Loss due to sol formation by particle diffusion

If the gel is not permitted to flow and smectite is lost solely by the diffusion of smectite particles from a rigid interface between gel and water, the loss of smectite can be approximately estimated using the Qeq concept. This was originally developed for diffusion of solutes from an interface between bentonite and water when the concentration at the interface as well as that in the approaching water is known (Neretnieks et al. 2010a). This could be relevant to a situation where the mobility of the particles is only governed by their thermal movement. The smectite loss N_{smect} is obtained from the carrying capacity of the water, called the equivalent flowrate Qeq, and the smectite volume fraction at the interface $\phi_{interface}$. The mass loss is obtained by multiplication with the smectite density.

$$N_{smect} = Q_{eq} \cdot \phi_{interface} \tag{6-1}$$

where

$$Q_{eq} = 4.5\delta\sqrt{D_{smect}\, r_{int}\, u} \tag{6-2}$$

The expression above assumes that the gel/water interface is at the radius r_{int}. The diffusivity of smectite particles is estimated by

$$D_{smec} = \frac{k_b T}{3\pi\eta d_p} \tag{6-3}$$

This is the Stokes-Einstein equation which is valid for large spherical molecules (or particles) in low molecular weight solvents (Bird et al. 2002)

For a smectite particle, d_p=0.3 mm in water at room temperature $D_{smec}=5\cdot10^{-13}$ m^2/s. This is 3–4 orders of magnitude less than that for small molecules.

Taking the smectite volume fraction at the gel/water interface 2% the rate of loss of smectite for the highest flowrate 315 m/yr is 0.016 kg/year. This is more than one order of magnitude less than what a flowing fluid could carry.

7 Impact of gravity on smectite loss

In appendix H some experiments are described, discussed and analysed where gravity effects were found to have a strong influence on the release of smectite in downward facing fractures. Our dynamic model, which quantifies bentonite expansion and colloid release accounts for gravity acting on the colloidal particles in the gel and sol. The observed effects are very much larger than what the model predicts. The reasons for these effects are not understood and no quantitative model based on fundamental principles has been devised. The observed release rates in narrow slits suggest that several tens of grams per year of MX-80 bentonite could be released in 1 mm aperture fractures. In other experiments with purified homoionic experiments in test tubes more than 100 times larger release fluxes were observed.

8 Discussion and conclusions

The smectite in the compacted buffer in the deposition hole expands out into fractures that intersect the deposition hole. In low ionic strength waters below the critical coagulation concentration the gel can release colloidal smectite particles into the seeping water, which can carry them away as a dilute sol. In addition, the dilute gel, before it actually becomes a sol, can flow downstream. The gel/sol viscosity is strongly influenced by the volume fraction of smectite and by the ion concentration in the pore water. A higher volume fraction of smectite in the gel/sol increases the viscosity. In addition when the ion strength is low the particles behave as if they are much larger because the electrical diffuse layer surrounding the particles increases the volume that they effectively occupy. The effect is quite strong in the region of interest.

The simulations show that the gel will flow with a non-negligible flowrate when its volume fraction is around one percent, but that the erosion and loss of smectite is not much influenced by the concentration of sodium in the clay or in the approaching seeping water. The latter effect is at first somewhat surprising but is caused by the combined effects of expansion force and viscosity as influenced by ion concentration. A lower ion concentration gives rise to larger expansion force but it is compensated by the higher viscosity.

The model for smectite expansion is based on the forces generated between particles by double layer expansion mediated by friction of the individual particles against the water that passes in the opposite direction as the gel expands. It can be likened to two gases or liquids mixing by molecular diffusion in a constant volume vial where part of the vial is filled with pure water and the other with water with a dye. The differences are that smectite particles are larger than at least small dye molecules and that the smectite particles exert strong repulsion forces between them. We thus neglect any distortion of the diffuse double layer by the relative movement between particles and water. The presence of walls of a fracture will have negligible influence on the process as long as the separation between the walls much larger than the smectite particles. This implies that pure smectite will expand into fractures at a rate that is independent of the fracture aperture. This is probably not true for a bentonite gel that also contains much larger particles of different accessory minerals.

The simulations in a rectangular slit and in slit with a circular geometry describing the interface between the compacted clay and the fracture give similar results both qualitatively and quantitatively although the latter case is more realistic. The simplified rectangular geometry has been useful for setting up the more complex circular geometry because the numeric schemes used then were computationally considerably more stable.

The results suggest that for the largest fracture transmissivities combined with the highest gradients will cause erosion by flow on the order of 0.3 kg per year. This is more than one order of magnitude larger than what only particle diffusion could cause.

It should be stressed that the modelling assumes that there are no other larger non-smectite particles that would be left behind to gradually build up a bed of particles that could act as filter, slowing down or even straining further smectite penetration into the fracture. The results could therefore be highly pessimistic because bentonites contain tens of percent of accessory minerals that do not form colloids and the presence of which may cause the expanding to be slowed down by friction against the fracture walls.

Experiments in downward facing slits (fractures) have been found to release swelling bentonite much faster than expected. The bentonite is released and sediments as gel agglomerates also under conditions where it is expected that the smectite particles should have separated into individual smectite sheets, which would not noticeably be influenced by gravity. The reasons for this behaviour are not understood.

References

SKB's (Svensk Kärnbränslehantering AB) publications can be found at www.skb.se/publications.

Adachi Y, Nakaishi K, Tamaki M, 1998. Viscosity of dilute suspension of sodium montmorillonite in an electrostatically stable condition. Journal of Colloid and Interface Science, 198, pp 100–105.

Bird R B, Stewart W E, Lightfoot E N, 2002. Transport phenomena. 2nd ed. New York: Wiley.

Birgersson M, Börgesson L, Hedström M, Karnland O, Nilsson U, 2009. Bentonite erosion. Final report. SKB TR-09-34, Svensk Kärnbränslehantering AB.

Jönsson B, Åkesson T, Jönsson B, Meehdi M S, Janiak J, Wallenberg R, 2009. Structure and forces in bentonite MX-80. SKB TR-09-06, Svensk Kärnbränslehantering AB.

Liu L, 2010. Permeability and expansibility of sodium bentonite in dilute solutions. Colloids and Surfaces A: Physicochemical and Engineering Aspects, 358, pp 68–78.

Liu L, Moreno L, Neretnieks I, 2009a. A dynamic force balance model for colloidal expansion and its DLVO-based application. Langmuir, 25, pp 679–687.

Liu L, Moreno L, Neretnieks I, 2009b. A novel approach to determine the critical coagulation concentration of a colloidal dispersion with plate-like particles. Langmuir, 25, pp 688–697.

Liu L, Neretnieks I, 2008. Homo-interaction between parallel plates at constant charge. Colloids and Surfaces A: Physicochemical and Engineering Aspects, 317, pp 636–642.

Neretnieks I, Liu L, Moreno L, 2009. Mechanisms and models for bentonite erosion. SKB TR-09-35, Svensk Kärnbränslehantering AB.

Neretnieks I, Liu L, Moreno L, 2010a. Mass transfer between waste canister and water seeping in rock fractures. Revisiting the Q-equivalent model, SKB TR-10-42, Svensk Kärnbränslehantering AB.

Neretnieks I, Liu L, Moreno L, 2010b. Diffusion of sodium and calcium in smectite gel – Impact on concentration at gel/water interface by ion exchange processes. Chemical Engineering and Technology, Royal Institute of Technology, KTH Stockholm Sweden. Report in preparation.

Appendix A

A simplified model to estimate the release of bentonite into the seeping water

The bentonite contains mostly colloidal size smectite particles. We model their migration. In our model the bentonite release from a fracture intersecting the deposition hole is described by three coupled partial differential equations. The equations are the water flow (Darcy equation), the smectite particle mass balance (Advection-diffusion equation for particles) and the counterion mass balance (Advection-diffusion equation for ions). The three coupled equations are solved in two dimensions by using Multiphysics (Comsol, version 3.5). The solution is time consuming and in some cases unstable. Therefore, a simplified, much faster solution was also developed solving the equations in one dimension only.

Simulations with the two-dimensional model showed that the flow of the gel/sol containing more smectite than a volume fraction about 0.02 was very small and could be neglected. See Chapter 4. This is because the viscosity of the suspension increases very rapidly with increasing smectite content slowing down the flow immensely. Most of the release takes place in a thin region close to the gel/water interface.

It was also found that the concentration and diffusion of the counterion did not influence the results much although the counterion, modelled as sodium has a strong influence on the viscosity of the suspension.

The simplified one-dimensional model

The simplified model neglects the counterion diffusion and sets the counterion concentration to a constant value. The smectite particles are allowed to migrate only in the y-direction perpendicular to the one dimensional source boundary out into the seeping water, which flows in the x-direction. The water velocity far from the source is constant and is determined by the hydraulic gradient and the fracture transmissivity. Nearer the smectite source the water is slowed down in the x-direction as its viscosity increases due to the presence of the smectite.

We thus neglect the suspension flow in the y-direction, which must result when the velocity in the x-direction changes.

The general equation for the bentonite expansion and flow neglecting the gravity forces is (Equation 2-4)

$$\frac{\partial \phi}{\partial t} = -\vec{u}\nabla\phi + \nabla\cdot\left(\frac{\chi}{f}\nabla\phi\right)$$

When the smectite diffusion only is in the y-direction and the flow only is in the x-direction the above equation simplifies to

$$\frac{\partial \phi}{\partial t} = -\frac{u(\phi=0)}{x_L}\cdot\frac{\eta(\phi=0)}{\eta(\phi)}\cdot\phi + \frac{\partial}{\partial y}\cdot\left(\frac{\chi}{f}\frac{\partial \phi}{\partial y}\right)$$

We implicitly assumed that

$$\frac{\partial \phi}{\partial x} = -\frac{\phi}{x_L}$$

and

$$u = u(\phi=0)\cdot\frac{\eta(\phi=0)}{\eta(\phi)}$$

where $u(\phi=0)$ is the velocity of smectite free water far away and x_L is the length of the fracture in the water direction. $\eta(\phi=0)/\eta(\phi)$ is the ratio between the viscosity of the smectite free water and that of the gel/sol with smectite.

The equation above was solved for the steady state, i.e. $\partial\phi/\partial t=0$ by using the software Multiphysics (Comsol, version 3.5).

Once the equation is solved, the release of bentonite into the flowing water is calculated. The results are shown in Table A-1 for sodium concentrations in the water of 1.0 and 10.0 mM. The results are compared with the release obtained from the 2-D rectangular model with a sodium concentration of 10 mM in the inner boundary (deposition hole) and 0.1 mM far away in the seeping water. Differences of about 25% are obtained.

Table A-1. Bentonite release for the one-dimensional model compared with the two-dimensional model. Front distance is the distance where the smectite volume fraction is almost zero. The smectite volume fraction at the source (inner boundary) is 0.40. x_L is 1.0 m in the simulations.

Water velocity,	2-D bentonite release/ front distance [1)]	Release, m^3/s m /front distance for c=1.0 mM	Release m^3/s m /front distance for c=10.0 mM	Error in release rate, %
$3.0 \cdot 10^{-7}$ m/s	1.33 10^{-13}, m^3/s m	$1.06 \cdot 10^{-13}$	$1.05 \cdot 10^{-13}$	20
9.15 m/yr	2.3 m	3.00 m	2.83 m	
$100 \cdot 10^{-7}$ m/s	8.46 10^{-13}, m^3/s m	$6.13 \cdot 10^{-13}$	$6.09 \cdot 10^{-13}$	28
315 m/yr	0.4 m	0.51 m	0.49 m	

1) Na concentration 10.0 mM at the bottom and 0.1 mM at the upper boundary.

Appendix B

A simplified model using a constant diffusion coefficient

The expansion of the smectite particles in the gel/sol is due to the strong repulsion forces between the particles. The expansion force is counteracted by the friction between the particles in the water. The rate of change in particle concentration can be described by a partial differential equation similar to the diffusion equation for small solutes such as ions. A main difference is that for the smectite particles the diffusivity is very dependent on the concentration of particles as well as of the ionic strength. This makes the equation very nonlinear in some regions. We call this diffusivity the Diffusivity function. However, in over a large region of interest i.e.$0.003 < \phi < 0.3$ and sodium concentration c<1 mM the Diffusivity function is fairly constant. This is the region where most of the expansion and smectite diffusion and gel/sol flow take place.

Figure B-1 is taken from Figure 6.15 in Neretnieks et al. (2009). The figure shows the Diffusivity function as a function of the bentonite volume fraction for smectite sheets of 300 nm in diameter for sodium concentration between 0.01 and 100 mM. The thickness of the smectite sheet is 1 nm and the charge density of –0.131 C/m^2. It is seen that the Diffusivity function is almost constant for a large interval of bentonite volume fraction if the ion strength is below 1 mM. The Diffusivity function is about $1.0 \cdot 10^{-09}$ m^2/s in this interval.

For a constant value for the Diffusivity function the equation of the Diffusivity function, $\frac{\chi}{f}$, the PDF (partial differential equation) for smectite expansion, again neglecting gravity, simplifies to

$$\frac{\partial \phi}{\partial t} = \frac{\chi}{f} \frac{\partial^2 \phi}{\partial x}$$

The release of bentonite into the passing water is now calculated solving the equation for the expansion of the smectite for a constant value of the Diffusivity function, the equation of diffusion of the ion, sodium in this case, and the Darcy equation for the water flow.

Table B-1 shows the results and they are compared with the case with variable Diffusivity function (See chapter 4). Considering the simplifying assumptions the agreement is fairly good when a value of $1 \cdot 10^{-9}$ m^2/s for the Diffusivity function is used. The differences are 48% for the case with the largest water velocity (315 m/yr) and about 22% for the case with a water velocity of 9.15 m/yr).

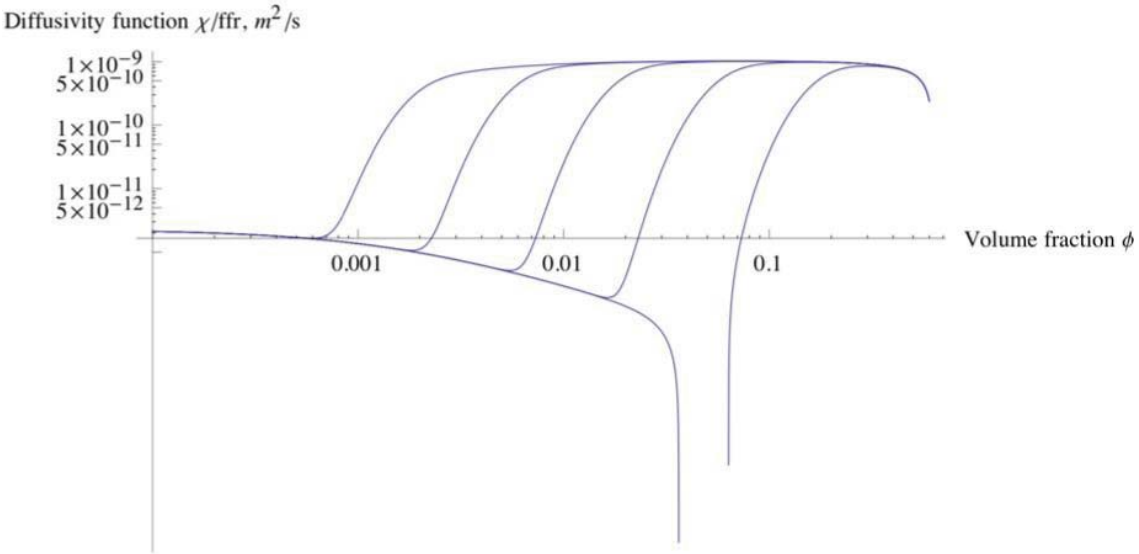

Figure B-1. *Diffusivity function for smectite 300 nm diameter sheets for monovalent ions. The curves from left to right are for 0.01, 0.1, 1, 10, 50 and 100 mM.*

Table B-1. Bentonite release when a constant Diffusivity function is used in the diffusion equation instead of the expansion equation. The calculations were done for the rectangular geometry.

Water velocity,	2-D bentonite release, /Front distance [1)]	Release rate for χ/f $1{\cdot}10^{-9}$ m²/s	Front distance for χ/f $1{\cdot}10^{-9}$ m²/s
$3.0{\cdot}10^{-9}$ m/s	$1.33{\cdot}10^{-13}$ m³/s m	$1.79{\cdot}10^{-13}$ (22%)	
9.15 m/yr	2.3 m		1.8 m
$30.0{\cdot}10^{-9}$ m/s	$4.61{\cdot}10^{-13}$ m³/s m	$6.08{\cdot}10^{-13}$ (32%)	
91.5 m/yr	0.7 m		0.6 m
$100.0{\cdot}10^{-9}$ m/s	$8.46{\cdot}10^{-13}$ m³/s m	$12.5{\cdot}10^{-13}$ (48%)	
315 m/yr	0.4 m		0.32 m

1) Na concentration 10.0 mM at the bottom and 0.1 mM at the upper boundary.

Considering the uncertainties in many of the parameters the error introduced by using a constant value of the Diffusivity function may well be acceptable. Tuning the value can be made to reduce the error further. The numerical solution is somewhat more stable using the constant value.

References

Neretnieks I, Liu L, Moreno L, 2009. Mechanisms and models for bentonite erosion. SKB TR-09-35, Svensk Kärnbränslehantering AB.

Appendix C

Impact on the bentonite release of the bentonite volume fraction at the fracture mouth

In the simulations, we have found that the release of bentonite into the flowing water is controlled by the bentonite concentration profile near the gel/water interface where the volume fraction is less than a few percents. Near the deposition hole the volume fraction is so large that the large gel viscosity effectively hinders the gel to flow. The gel/sol flows only at volume fractions below a few percents. It is therefore expected that the rate of loss of smectite will not be much influenced by the smectite volume fraction at the mouth of the fracture. The volume fraction near the deposition hole will mainly influence how far out from the mouth of the fracture the gel/sol front stabilises at steady state. This is for the case when the gel expansion only takes place in one dimension. For the two dimensional expansion, as is the case for the cylindrical source around the deposition hole, this is not quite the case because the gel expands radially and the contact surface circumference of the gel/sol/water interface increases. Nevertheless, the impact of the volume fraction at the source is not very large as is demonstrated below.

Simulations were performed using different values of volume fraction at the fracture mouth. Table C-1 shows the release of bentonite and the location of the gel/water interface where the bentonite is released into the flowing water. The simulations were made for the rectangular geometry with the full two-dimensional model including also counter ion (sodium) migration.

From the results shown in Table C-1 and also in Figure C-1, it is seen that for high concentrations at the boundary the release is constant. When the volume fraction at the fracture mouth is 0.20 a small decrease is observed. A volume fraction of 10% means that more than 80% of the smectite originally in the deposition hole has been lost. For a volume fraction at the fracture mouth of 0.05 the decrease of the release is considerable. Figure C-2 shows the location of the gel-water interface.

Table C-1. Bentonite release and location of the gel-water interface for different bentonite volume fractions at the fracture mouth. The simulations were made for a water velocity of 9.45 m/yr using the rectangular geometry.

Bentonite volume fraction	Relative release	Distance to the front, m
0.60	0.99	2.86
0.40	1.00	2.38
0.20	0.92	1.48
0.10	0.71	0.76
0.05	0.29	0.21

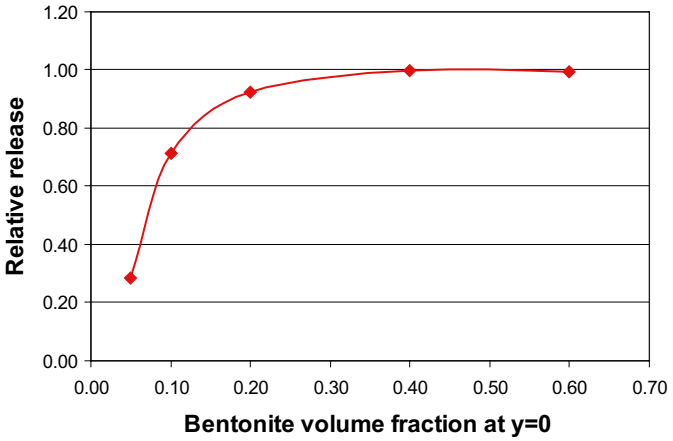

Figure C-1. *Smectite release as a function of the bentonite volume fraction at the lower border.*

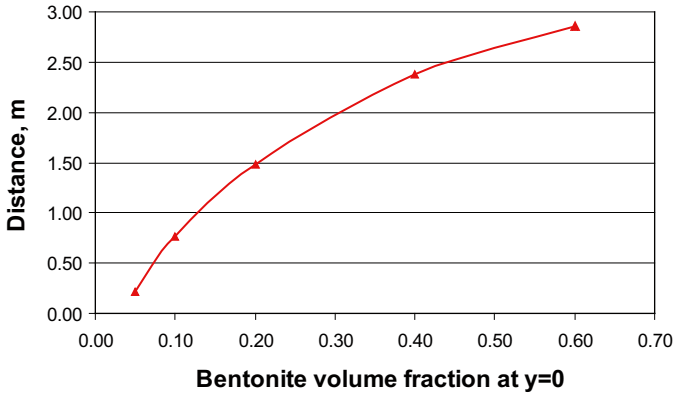

Figure C-2. *Distance of the gel-water interface as a function of the smectite volume fraction at the lower border.*

Figures C-3 and C-4 show the smectite concentration profile in the fracture. The differences at the interface are possibly due to different cation concentrations in the interface since the cation has to travel different distance through the smectite gel. At the lowest smectite concentration at the border the travel distance through the smectite is smallest, therefore, it may be expected that the cation concentration is higher. This could also explain the differences in the smectite release; expansive forces are smaller at smectite volume fractions of a few percent and sodium concentration about 10 mM.

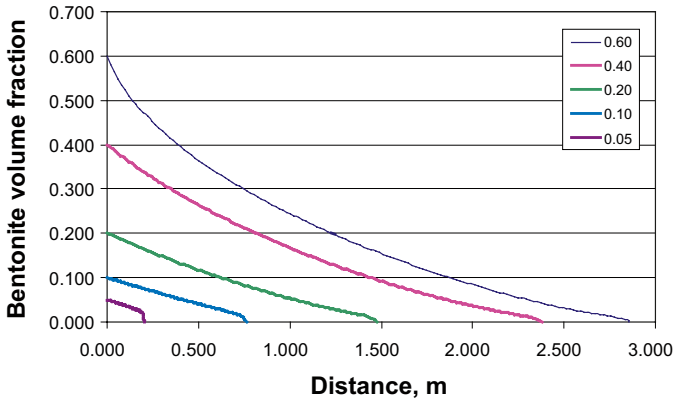

Figure C-3. *Smectite volume fraction profiles for different concentrations at the border.*

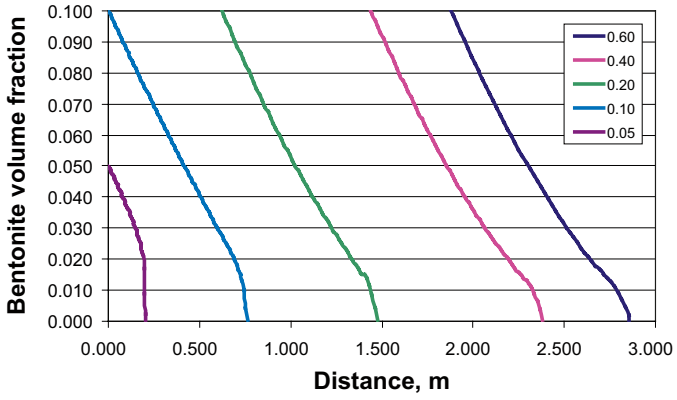

Figure C-4. *Smectite volume fraction profiles for different concentrations at the border. Enlargement of the zone close to the interface.*

Appendix D

Impact of the relation used for describing the gel viscosity

In the calculations performed in the report, it was found that the velocity of the fluid drops considerably where the smectite volume fraction is larger than a few %. This is due to the strong increase in viscosity with increasing smectite volume fraction. Here we explore a case where the gel viscosity abruptly becomes so large that the gel entirely stops flowing above a certain volume fraction.

The flow of the fluid (gel/sol/water) in the fracture is modelled by the Darcy equation where the gel/sol/water is considered as a fluid with viscosity varying with smectite volume fraction and ion concentration in the pore water. The viscosity of the fluid increases rapidly with increasing smectite volume fraction. For high smectite volume fractions, the viscosity is many orders of magnitude larger than that for the water and it becomes increasingly non-Newtonian. It is conceivable that even Bingham fluid type properties become important. A Bingham body/fluid needs a minimum shear stress to flow at all. Such effects have been observed (Birgersson et al. 2009) already at volume fractions below 1%.

Rheological data have been obtained for sodium-exchanged smectite over a wide range of smectite volume fractions (Birgersson et al. 2009). They show that the gels become increasingly more viscous and much more non-Newtonian at volume fractions above the percent level. Thixotropic effects (resting time of gel before stress is applied) also become increasingly more important at smectite volume fractions larger than about 1%. The use of a Newtonian viscosity model becomes increasingly unrealistic but we have found no viable alternative. We have chosen to extrapolate Equation (2-19) over the full range used in the simulations. This is defensible because the simulation results show that the gel will be so viscous at higher volume fractions that it will contribute very little to the transport of smectite due to gel flow.

Here, we test the implications of this assumption of a Bingham body/fluid on the smectite release into the flowing water. We assume that the water gel velocity is zero for smectite volume fractions greater than 0.02 using the rectangular geometry. For a water flow rate of 9.5 m/yr, the results show that the release of smectite is decreased by about 25%. It is also seen that the intrusion of the gel-water interface reaches a larger distance. The smectite concentration profiles are shown in Figure D-1.

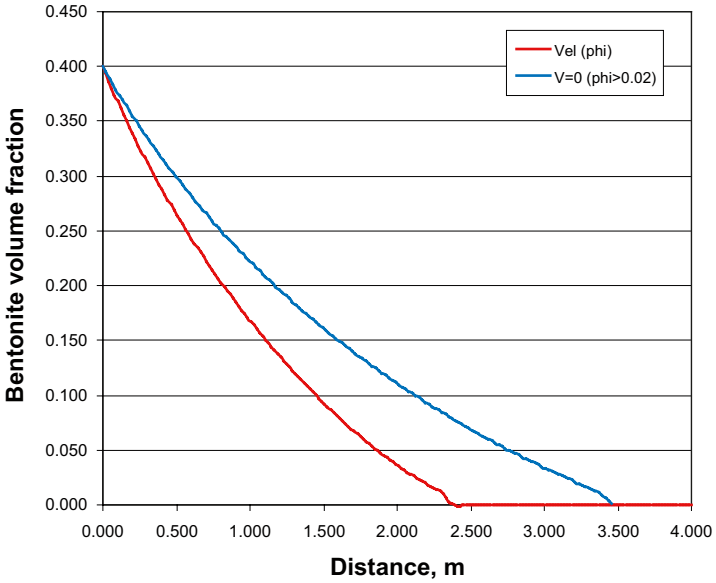

Figure D-1. *Smectite volume fraction profiles for the case where the viscosity is extrapolated for high smectite concentrations and the case where it is assumed that the gel/water velocity is zero if the smectite volume fraction is greater than 0.02.*

References

Birgersson M, Börgesson L, Hedström M, Karnland O, Nilsson U, 2009. Bentonite erosion. Final report. SKB TR-09-34, Svensk Kärnbränslehantering AB.

Appendix E

Impact of cation (sodium) concentration on the smectite release

The simulations for the rectangular geometry using the full two-dimensional model were made using a concentration for the sodium of 10 mM in the smectite in the deposition hole (fracture mouth) and 0.1 mM in the seeping water in the fracture far away from the bottom boundary.

In order to tests the sensitivity of the sodium concentration on the smectite release into the flowing water some calculations were made using different sodium concentrations. Table E-1 shows the relative release for different sodium concentration in the smectite and water in the fracture. The results are for the case with a water velocity of 94.5 m/yr and rectangular geometry. Figure E-1 shows the results graphically.

Table E-1. Smectite release for different sodium concentrations in the smectite and fracture water.

Sodium concentration at the smectite and flowing water, mM	Relative release
10 – 0.1	1.00
100 – 1.0	0.91
100 – 10	0.83

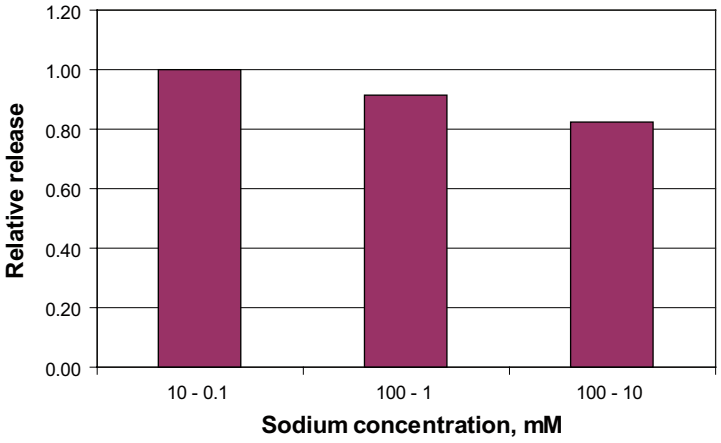

Figure E-1. *Smectite release for different sodium concentrations in the smectite and fracture water.*

Appendix F

Impact of the hole diameter (tunnel, deposition hole, borehole) on the smectite release

The calculations for a cylindrical geometry were made for a deposition hole with a diameter of 1.75 m. Here we present results for two other cylinder diameters. Figures F-1–F-3 show the smectite intrusion into the fracture for source diameters of 0.5, 1.75, and 5.0 m. The simulations were made for a water velocity of 9.45 m/yr. Observe that the scales in the figures are different.

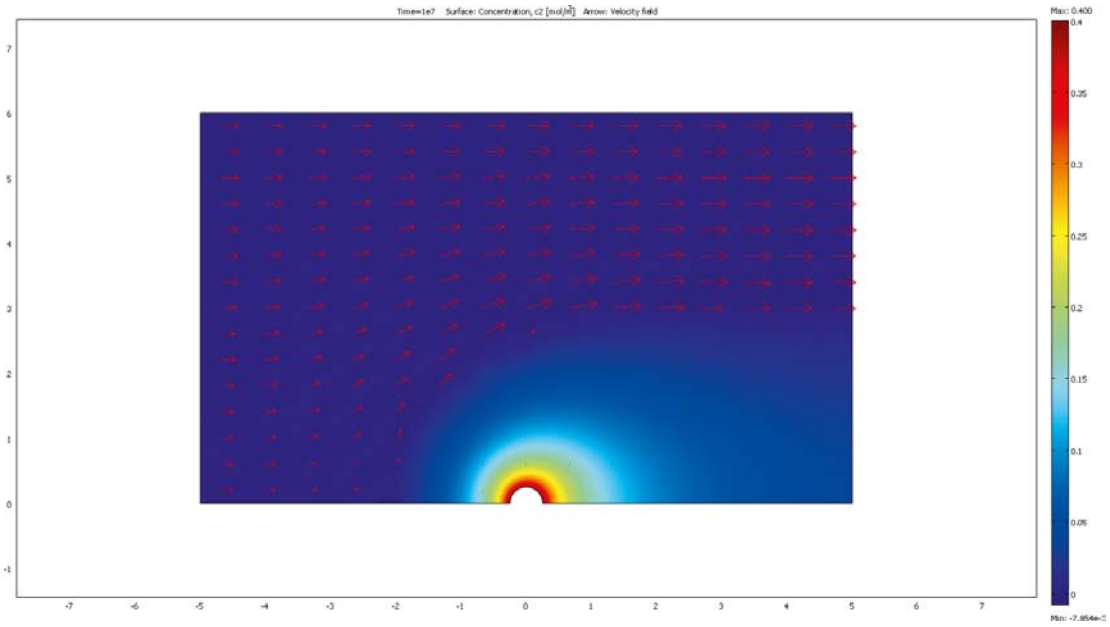

Figure F-1. *Smectite release for a source diameter of 0.5 m.*

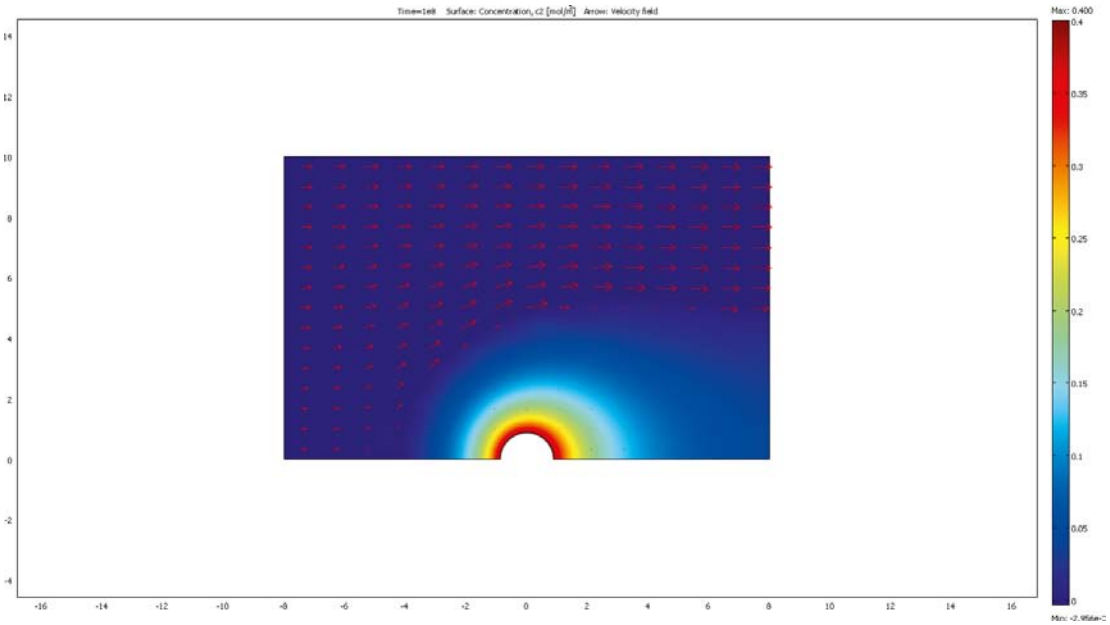

Figure F-2. *Smectite release for a source diameter of 1.75 m.*

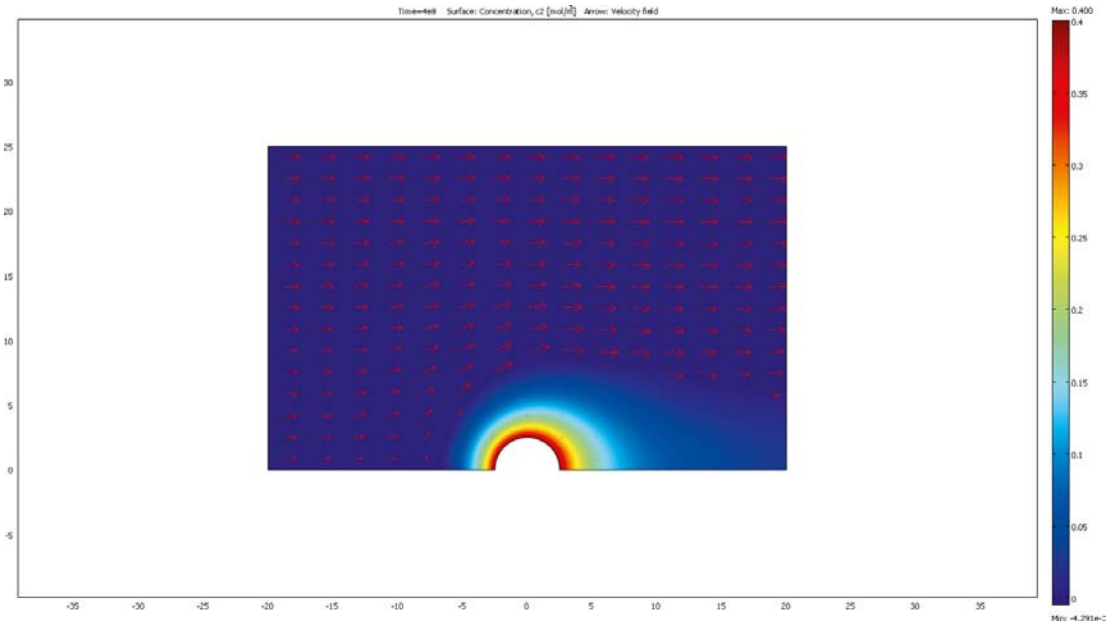

Figure F-3. Smectite release for a source diameter of 5.0 m.

The smectite release rate is show in Figure F-4 as a function of the water velocity in the fracture far away from the deposition hole and for three different diameters: 0.5, 1.75, and 5.0 m. The release increases with the hole diameter.,

The larger diameter increases the smectite erosion rate by less than a factor 2. The smaller hole decreases the smectite erosion rate by about a 30%.

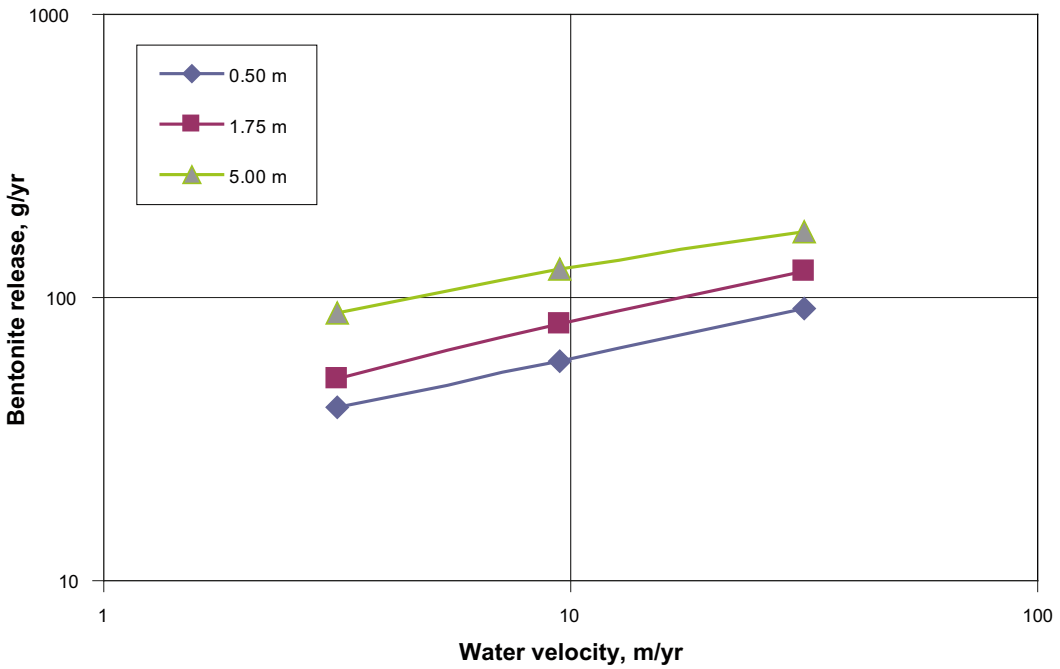

Figure F-4. Smectite release as a function of the water velocity for different source diameter.

Appendix G

Relations between fracture transmissivity and flow velocity in a fracture network

In Chapter 5, the release rate of smectite is calculated for different fracture transmissivities. The calculations were made for a hydraulic gradient of 0.1 (m/m) applied to an individual fracture with a fracture aperture of 1.0 mm and for a deposition hole diameter of 1.75 m.

For a given geometry the erosion rate is proportional to the fracture aperture and the water velocity to an exponent of about 0.4 so that a simple scaling can be used once the aperture that intersects the deposition hole and the water velocity in it is known.

The fracture transmissivity and the fracture aperture are correlated and we describe three such relations. Furthermore the flowrate in a fracture within a network of fractures is not proportional to the individual fracture transmissivity and global gradient because fractures with large transmissivities most often connect to fractures with low transmissivities. The low transmissivity fractures will determine the flowrate that can enter the high transmissivity fracture. In this appendix we explore this effect.

Transmissivity-aperture relationship

Fractures with small apertures usually have small transmissivities. A common relationship is the cubic law, which relates the transmissivity to the aperture of an idealised, perfect parallel-plate aperture,

$$e_h = \sqrt[3]{\frac{12 \cdot \mu \cdot T}{\rho \cdot g}} = \left(\frac{12 \cdot \mu}{\rho \cdot g} \right)^{1/3} \cdot T^{1/3} \qquad \text{(G-1)}$$

e_h is the hydraulic aperture, T transmissivity, μ water viscosity, ρ water density and g the gravitational constant. The hydraulic aperture is smaller than the actual mean physical fracture aperture in real fractures with rough variable aperture. Fractures also may contain infill of small particles, which increase the flow resistance. For fractures filled with small particles, e.g. clays, the transmissivities will be proportional to the aperture.

Therefore, the exponent in the relationship between hydraulic aperture and transmissivity can be expected to vary from 1/3 to 1.0. In some field experiments the exponent has been found to be around ½ (Sawada et al. 2001, Dershowitz et al. 2003). A more general expression is

$$e_h = a \cdot T^b \qquad \text{(G-2)}$$

where a and b are experimentally fitted parameters. For the TRUE Block Scale project (Dershowitz et al. 2003) the parameter values are: a = 0.46 mm and b = ½, then T has units m^2/s. The parameter values determined by Sawada et al. (2001) are: a = 3.15 and b = ½. For the cubic law, the fracture aperture may be calculated directly from Equation (G-1). If this equation is used the values for the parameters are a = 0.01075 and b = 0.333.

Figure G-1 shows the relationships for fracture aperture as a function of fracture transmissivity for the three cases. The figure shows that if the Sawada et al. relationship is used, larges values for fracture aperture are obtained for large fracture transmissivities. The fracture aperture is about 3 mm for transmissivity of $1 \cdot 10^{-6}$ m^2/s. The smallest values are found when the cubic law is used.

The water velocity in the fracture is determined from the fracture transmissivity, the hydraulic gradient, and the fracture aperture as shown in Equation (G-3).

$$\vec{u} = \frac{T \cdot \vec{i}}{\delta} \qquad \text{(G-3)}$$

The water velocity is plotted in Figure G-2 for the three cases for a hydraulic gradient of 0.1 m/m. The largest water velocities in the fracture are obtained for the case where the cubic law is used. Extremely high values (tens of kilometres per year) are obtained for the water velocity for fracture transmissivity of $1 \cdot 10^{-6}$ m^2/s. Even for the case where the Dershowitz et al. (2003) relationship is used, the water velocity reaches very high values. Figure G-3 shows the fracture aperture as a function of the water velocity for different relationship between fracture transmissivity and fracture aperture for a hydraulic gradient of 0.1 m/m.

It is seen that the fracture aperture is not well known and there will be a considerable uncertainty in assessing the erosion rate of smectite, especially for the more transmissive fractures.

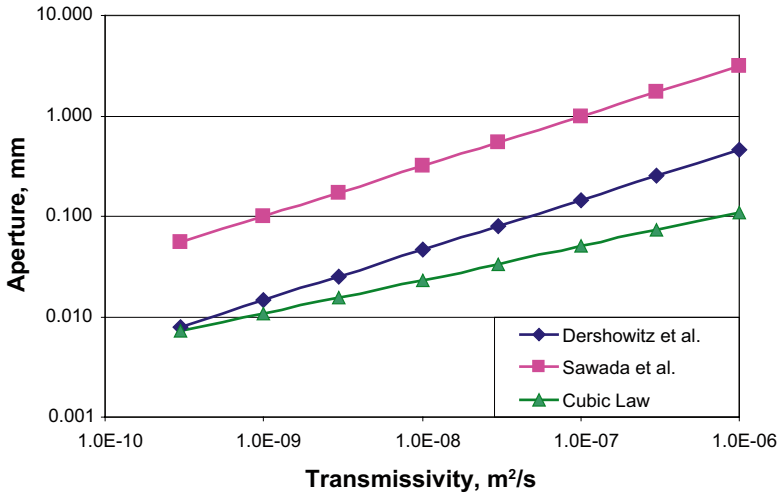

Figure G-1. *Aperture as a function of the transmissivity for different relationship between fracture transmissivity and fracture aperture.*

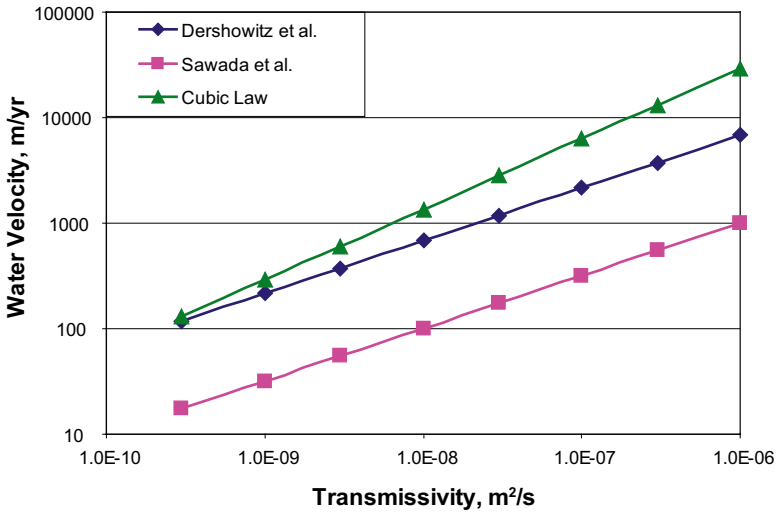

Figure G-2. *Water velocity as a function of the transmissivity for different relationships between fracture transmissivity and fracture aperture for hydraulic gradient of 0.1 m/m.*

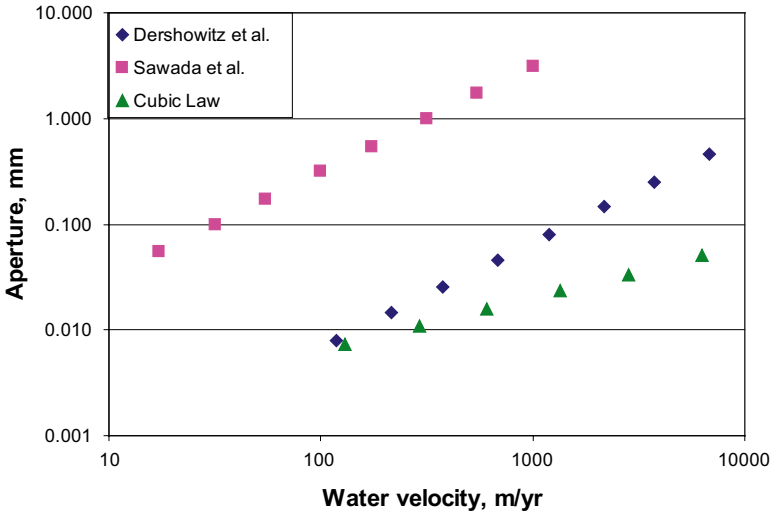

Figure G-3. *Fracture aperture as a function of the water velocity for different relationship between fracture transmissivity and fracture aperture for a hydraulic gradient of 0.1 m/m.*

Flowrates in fractures in a network

For a network of connected fractures it is expected that the local hydraulic gradient is lower than the regional hydraulic gradient in fractures with large transmissivities because the pressure drop will occur in the low transmissivity fractures connected to the high transmissivity fracture. Therefore it is expected that the water velocity in the fractures with high transmissivity around the canister deposition hole will be much lower than the values shown in Figure G-2.

Figures G-4 and G-5 show results of simulations made using the channel network model (Gylling et al. 1999). In CHAN3D the fractures are modelled as channels with a given width. Log-normal distributions for channel conductance (transmissivity×width) were used. Simulations of flowrate distributions were made for some large channel networks (64,000 channels) with log-normal distributions of conductances. The conductance of the channels, and the water flowrates and hydraulic gradients in each channel were recorded. The figures show the hydraulic gradient over individual channels plotted versus the channel conductance. The conductance is normalised to the mean conductance in the conductance distribution.

The results show that the hydraulic gradients over the channels with conductances below the mean vary around the global gradient 0.1. However, for channels with conductances larger than the mean the local gradient decreases strongly with increasing conductance. The slope of the line drawn approximately as a tangent to the swarm of points in the first quadrant is around 1 and intersects vertical gradient axis at around 10 for a relative conductance of unity, which is the mean conductance by which the data are normalized, in both figures. This suggests that even fractures with the highest transmissivities will not have higher flowrates than about 100 times of the flowrate in a fracture with the mean transmissivity exposed to the global gradient. Most of the very high transmissivity fractures will have much smaller flowrates as can be seen from the density of the swarm of points. This is shown in Figures G-6 and G-7, where the normalized water flowrate as a function of the channel conductances is plotted for both conductance distributions (0.8 and 1.6 in log10 scale).

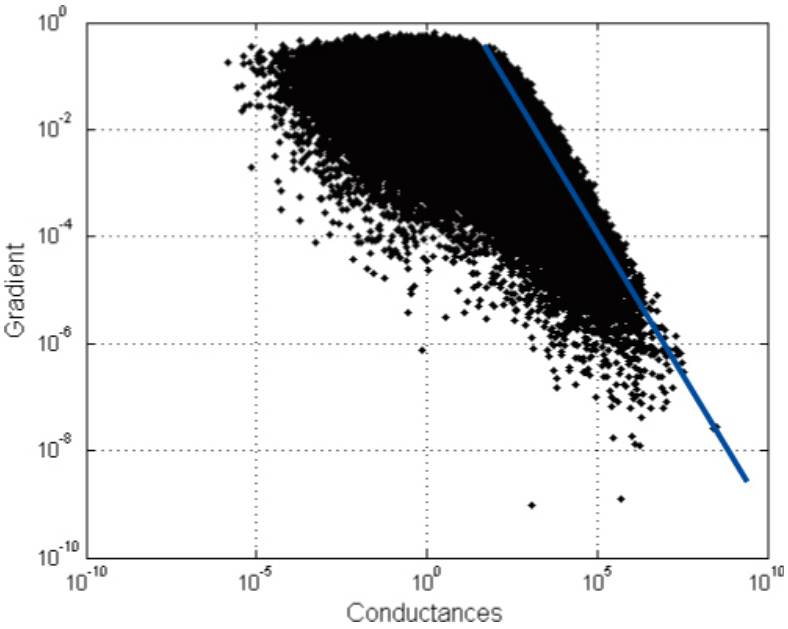

Figure G-4. *Hydraulic gradient as a function of the channel conductances for a channel network with a large standard deviation in conductance (1.6 in log10 scale). The regional gradient applied to the network was 0.1 m/m.*

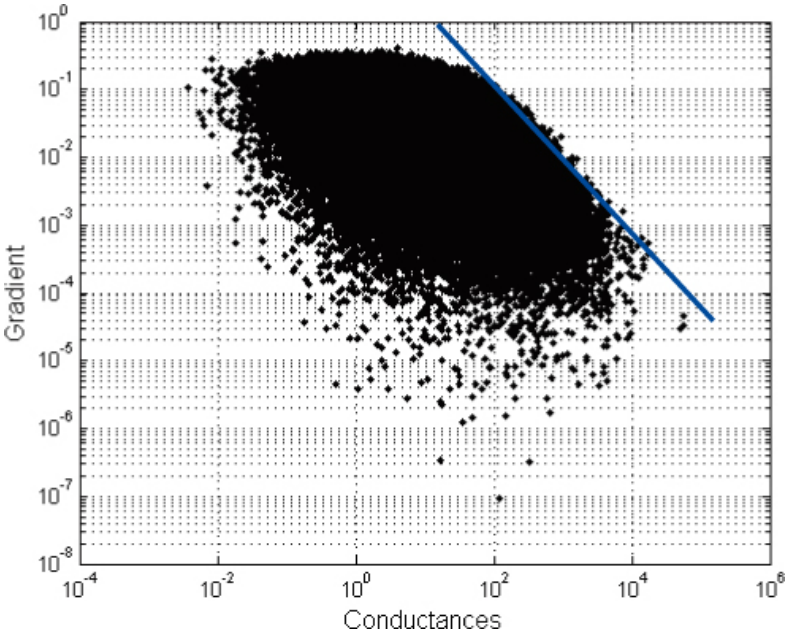

Figure G-5. *Hydraulic gradient as a function of the channel conductances for a channel network with a low standard deviation in conductance (0.8 in log10 scale). The regional gradient applied to the network was 0.1 m/m.*

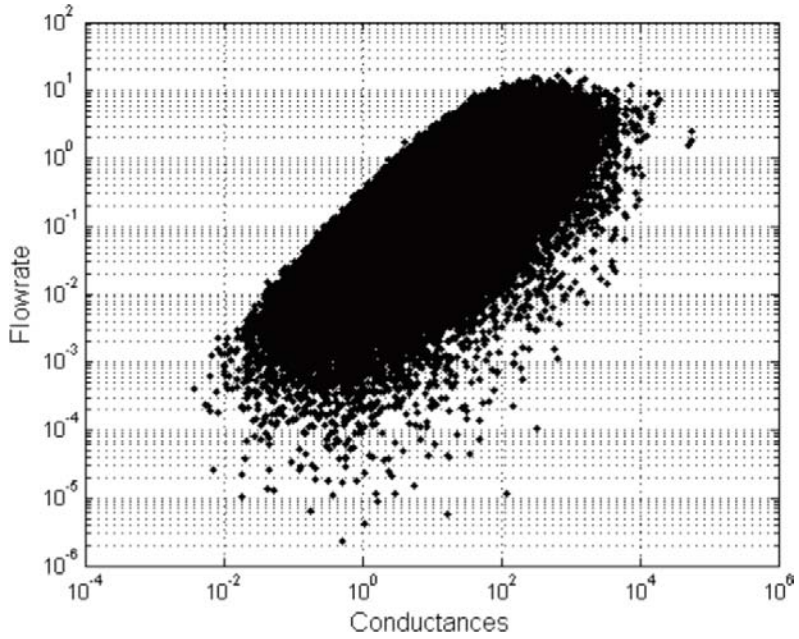

Figure G-6. *Normalized flowrate as a function of the channel conductances for a channel network with a low standard deviation in conductance (0.8 in log10 scale). The regional gradient applied to the network was 0.1 m/m.*

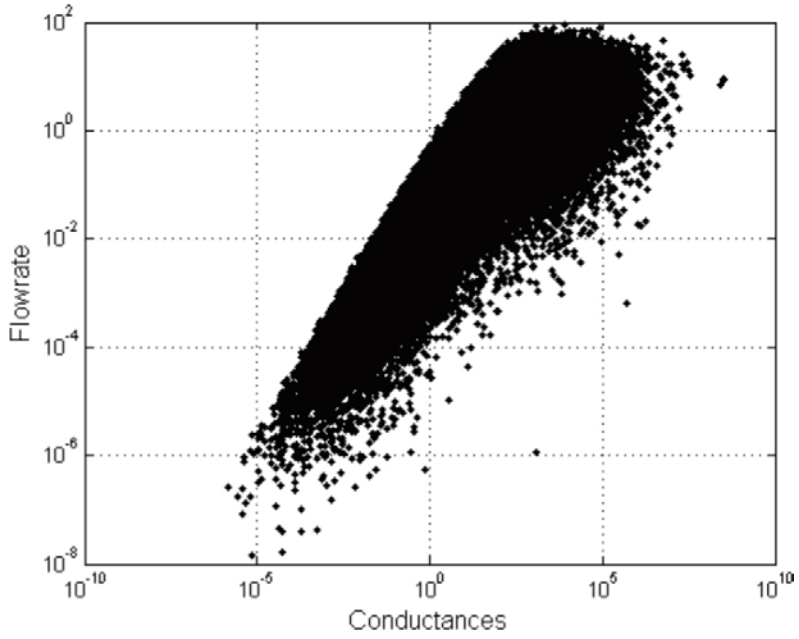

Figure G-7. *Normalized flowrate as a function of the channel conductances for a channel network with a low standard deviation in conductance (1.6 in log10 scale). The regional gradient applied to the network was 0.1 m/m.*

References

Dershowitz W, Winberg A, Hermanson J, Byegård J, Tullborg E-L, Andersson P, Mazurek M, 2003. Äspö Hard Rock Laboratory. Äspö Task Force on modelling of groundwater flow and transport of solutes. Task 6c. A semi-synthetic model of block scale conductive structures at the Äspö HRL. SKB IPR-03-13, Svensk Kärnbränslehantering AB.

Gylling B, Moreno L, Neretnieks I, 1999. The Channel Network model – a tool for transport simulations in fractured media. Ground Water, 37, pp 367–375.

Sawada A, Uchida M, Shimo M, Yamamoto H, Takahara H, Doe T, 2001. Anisotropy, reversibility and scale dependence of transport properties in single fracture and fractured zone – Non-sorbing tracer experiment at the Kamaishi mine. In: First TRUE Stage – Transport of solutes in an interpreted single fracture. Proceedings from the 4th International Seminar Äspö, September 9–11, 2000. SKB TR-01-24, Svensk Kärnbränslehantering AB, pp 151–164.

Appendix H

Gravity effects on erosion of bentonite

Abstract

Fully water saturated bentonite releases particles consisting of smectite and detritus material downward from the bentonite/water interface. This gravity-induced release has been observed in three different types of experiments, including into narrow slits. This could contribute to the erosion of bentonite from deposition holes for high-level nuclear waste. In one of the experiments the release rate is much larger than what presently available models predict. The release mechanisms are not understood and the release rates cannot be predicted based on available experiments, theories and models.

Background

We have developed a model for smectite expansion and contraction in low ionic strength water based on a force balance for forces between and on smectite particles including gravity. The model has been verified by a number of experiments (Neretnieks et al. 2009) with pure homoionic sodium smectite expanding upward against gravity (Dvinskikh and Furó 2009). However, other experiments where gravity pulls downward on an interface of smectite, e.g. in an upside down turned test tube with the smectite above a very fine net the smectite rapidly penetrates through the fine holes in the net and sediments downward (Jansson 2009). In other experiments in thin slits the same phenomenon was observed with natural bentonite containing calcium sulphate and detritus material and with a mixture of homoionic sodium smectite and purified detritus material (Neretnieks 2009). We wish to explore if this unexpectedly fast release and sedimentation of smectite in a downward facing fracture could cause a more rapid release of smectite from a deposition hole for a nuclide waste canister.

Some ideas on the causes of the rapid release and sedimentation of smectite

In our dynamic model (Neretnieks et al. 2009) we assume that the individual thin smectite sheets are fully separated or that the particles consists of stacks of parallel closely aligned sheets of smectite particles. Such particles are of colloidal size and sediment very slowly. In fact thermal movement (particle diffusion) dominates their behaviour. Even stacks made up of up to a few tens of individual sheets sediment very slowly (Neretnieks et al. 2009).

The rapid sedimentation can only be due to the presence of larger agglomerates of individual smectite sheets even if these occupy a small volume fraction in the agglomerate and their density is only slightly larger than that of water. Agglomeration is not expected in the low ionic strength waters used in the experiments because the double layer repulsion forces should hinder such agglomerates to form. It has been proposed that the smectite sheets can have positive edge charges that could cause them to form stacks or even form house of card type arrangements (Birgersson et al. 2009). In the experiments with the upside down turned test tubes the smectite was dispersed in distilled water by shaking and sonification before the tubes were turned upside down (Jansson 2009). The suspension looked homogeneous to the eye. It was rested for 24 hours before turning the tubes upside down. Then the smectite rapidly fell through the net with fine pores and sedimented.

Other observations in upside down turned slits with natural bentonite containing gypsum and detritus as well as homoionic smectite mixed with detritus material washed of soluble calcium salts (gypsum) reveal the formation of small “blobs” of smectite gel that slowly are released from the gel interface and sediment downward (Neretnieks 2009).

In some recent experiments in 1.3 mm wide slits between two glass plates dry smectite powder (well) mixed with purified detritus (small non-smectite minerals that are present in natural bentonite) was poured into the air filled vertical slit. Some small agglomerates did not fall all the way down to the bottom of the slit but were stuck between the plates. The aim of experiment was to observe how smectite expanded in water and how it leaves the larger detritus particles behind. After filling the slit with water the powder at the bottom started to swell as did the agglomerates stuck in the slit. These agglomerates slowly release very small particles that sedimented downward with a low but still visually observable velocity. It took up to a few days for these agglomerates to disperse fully. See Figures H-1 and H-2.

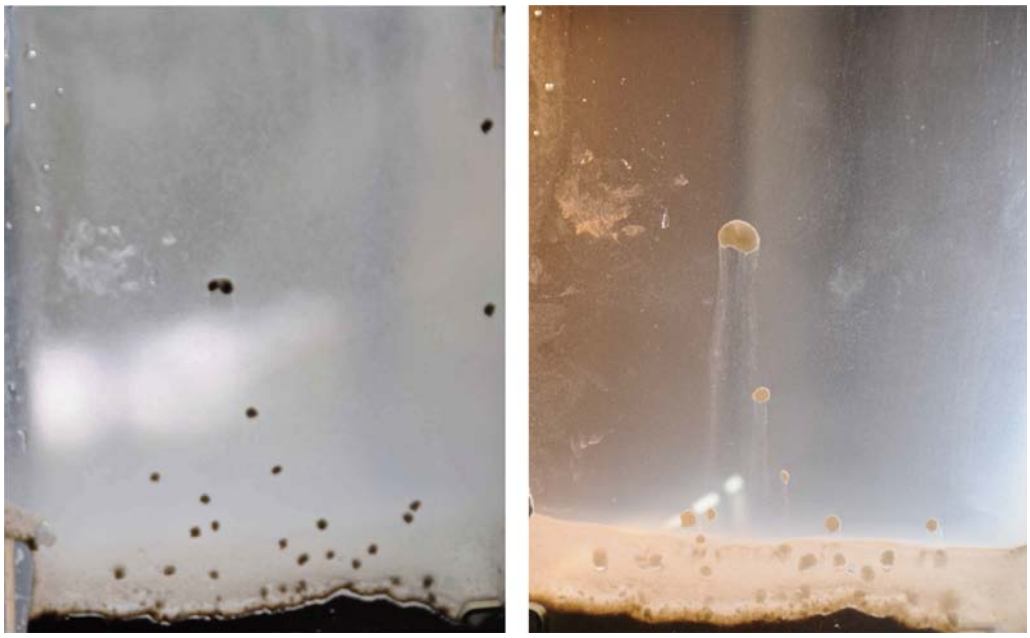

Figure H-1. *Agglomerates in the slit swell rapidly after water addition. Left picture taken a few minutes after water addition. Picture is 12 cm wide. Right picture taken about 2 hours later.*

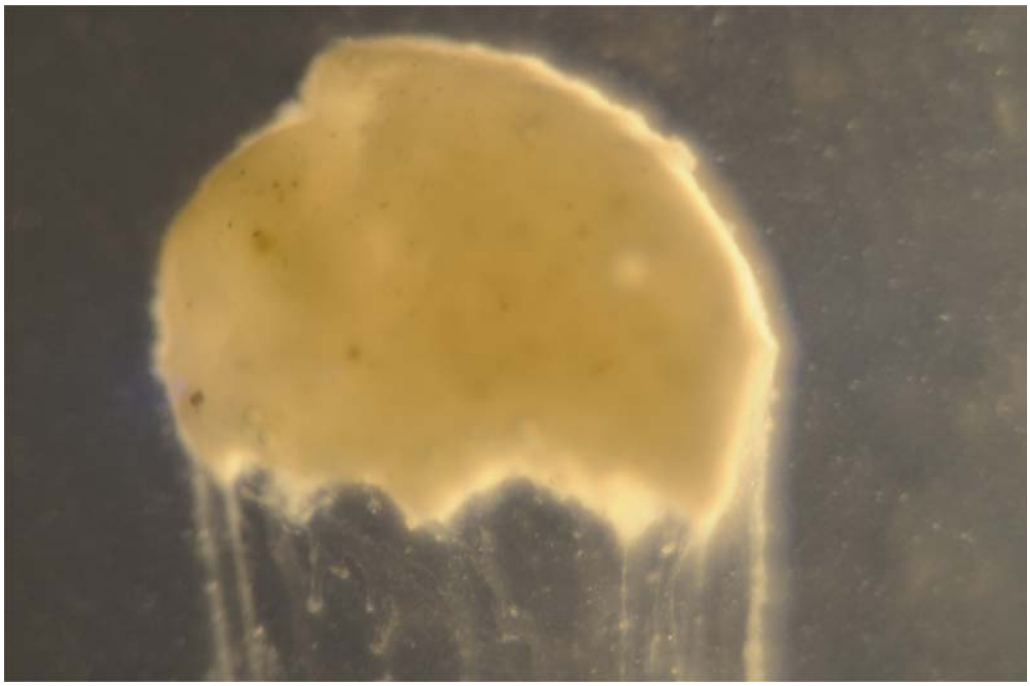

Figure H-2. *Disintegrating "blob" and sedimentation of small particles. Picture taken 4 hours after water addition. Blob size is about one cm in the picture and is 1.3 mm thick, the aperture of the slit.*

It may be noted that these observations do not contradict the validation of the dynamic model for expansion upward against gravity. Even if most of the particles form aggregates these still expand by the repulsion forces between the sheets. The whole system thus expands as the aggregates expand. Some sheets are still free and form the observed diffuse region at the gel/sol/water interface. The agglomerates are held close to each other by gravitation and because of their size they are not noticeably influenced by the thermal forces. Macroscopically the system behaves as if the agglomerates do not exist.

However, when the system is turned upside down the agglomerates, which are not held together, can detach themselves from each other and slowly fall downward because larger particles sediment more rapidly than small. This is commonly used in sedimentation separation processes by causing small particles to agglomerate by adding surface-active agents.

We do not know the reason for such large agglomeration in some of the systems studied that would be needed for the observed rapid sedimentation of agglomerates. Homoionic sodium smectite in essentially distilled water is observed to form very dilute sols although the colloid particles sizes may vary considerably.

Figures H-1 and H-2 show some examples of rapid sedimentation of agglomerates.

The "blobs" in this experiment did not move downward with a visible velocity. They had expanded against the sides of the glass plates and friction retards their movement. The smallest particles seen to sediment are on the order of 100 micrometer in diameter.

A possible reason in this case for the small particle sedimentation is that the detritus particles, which are mineral grains, pull or push the smectite particles that surround them downward.

Estimates of release rate

In the experiments reported by Jansson (2009) the test tube has a diameter of about 2.5 cm, which gives a cross section area of 5 cm^2. A mass of 0.2 g of homoionic smectite sedimented through the 17 mm mesh size net in about 10 minutes. The specific release rate, flux, of smectite is 0.24 g cm^{-2} $hour^{-1}$. In this experiment the smectite "blobs" were smaller than the diameter of the tube and they were probably not much influenced by wall friction. On the other hand they had no difficulty in rapidly wriggling through 17 mm openings.

This rapid release differs from what was observed in the experiments in the slits. In the experiment with untreated bentonite MX-80 in distilled water it took 0.106 g bentonite in a slit with 1.32 mm aperture and 13 cm long about 48 hours to be released and sediment (Neretnieks 2009). This corresponds to 0.0013 g cm^{-2} $hour^{-1}$. This is more than 100 times less than in the previous case. However, the "blobs" were several mm to a centimetre large and visibly could be seen to slowly change shape as they moved downward. This was interpreted as being caused by friction against the walls of the slit.

The dry clay aggregates that stuck between the glass plates were about 1 mm diameter. See Figures H-1 and H-2. It is estimated that they are roughly 1 mm^3 and have a mass of 1 mg. The particles rapidly swelled out in 2 dimensions to become about one cm across. The release took place from a cm length in a 1.3 mm wide slit. The "blobs" had essentially disappeared in 48 hours so the flux is about $1.6 \cdot 10^{-4}$ g cm^{-2} $hour^{-1}$. In this case wall friction is not deemed to have influenced the rate of disintegration of the blobs.

Should these release rates be representative of conditions around the canister deposition hole an estimate of the rate of loss of bentonite can be made. The diameter of the deposition hole is 1.75 m and its mean aperture is taken to be 0.1 mm. This gives an area for release of 1.75 cm^2.

With a release rate of 0.24 g cm^{-2} $hour^{-1}$ this gives a loss rate of 0.42 g $hour^{-1}$, equivalent to 3,700 g $year^{-1}$ or 3,700 kg per 1,000 years.

With a release rate of $1.3 \cdot 10^{-3}$ g cm^{-2} $hour^{-1}$ this gives a loss rate of 0.0023 g $hour^{-1}$, equivalent to 19.9 g $year^{-1}$ or 19.9 kg per 1,000 years.

With a release rate of $1.6 \cdot 10^{-4}$ g cm^{-2} $hour^{-1}$ this gives a loss rate of 0.00028 g $hour^{-1}$, equivalent to 2.5 g $year^{-1}$ or 2.5 kg per 1,000 years.

Discussion and conclusions

The upside down turned test tube experiment is not representative of repository conditions for several reasons. One reason is that the smectite used was homoionic and another reason is that the clay is essentially free of detritus material. There was probably negligible wall friction to slow down the sedimentation of agglomerates of the smectite particles which are loosely held together. These agglomerates can rapidly change their shape because they could rapidly penetrate the fine pores in the filter and probably recombine to larger agglomerates that "rapidly" sediment. The volume fraction of the first formed suspension in the 10 ml water is about 0.74%. This is still in the region where very strong repulsion forces between particles are expected in the very low ionic strength water in the experiment (Neretnieks et al. 2009). The mechanisms for recombination to larger agglomerates are not understood yet.

From the sedimentation velocity of the agglomerates their size can be estimated using Stokes's law. The stationary sedimentation velocity of a sphere is (Bird et al. 2002)

$$u_p = \frac{d_p^2(\rho_p - \rho_w)g_c}{18\eta_w}$$

d_p is the diameter of a sphere, r_p and r_w the densities of the agglomerate and water respectively, h_w water viscosity and g_c the gravitational constant. The observed velocity is on the order of 5–10 cm per ten minutes. The density of the agglomerate is estimated from the original volume fraction, 0.0074 to be 1.0125 g cm^{-3}. The Stokes' law diameter of the agglomerate is about 0.11 mm.

Such agglomerate sizes are of the same order of magnitude as the aperture of expected fractures in the rock. It thus, at present, cannot be ruled out that small enough smectite aggregates could be released and sediment in fractures and add to erosion. However, it is expected that the presence of fracture walls and variable aperture fractures will considerably decrease the rate of loss. In such fractures the agglomerates will have to slide or roll slowly along the fracture walls if the fracture is not absolutely vertical. Also when the agglomerate reaches a tight or closed section in the fracture it will have to change shape and move sideways to pass the restriction. Furthermore, agglomerates that carry detritus particles can be expected to release these when the smectite agglomerate changes shape to pass a narrow passage. Eventually the passages may be filled with detritus particles, which would further hinder agglomerates and also individual smectite sheet movement.

It is not at present possible to quantify these processes. Further experiments and model development are needed to understand and quantify these phenomena.

References

Bird R B, Stewart W E, Lightfoot E N, 2002. Transport phenomena. 2nd ed. New York: Wiley.

Birgersson M, Börgesson L, Hedström M, Karnland O, Nilsson U, 2009. Bentonite erosion. Final report. SKB TR-09-34, Svensk Kärnbränslehantering AB.

Dvinskikh S V, Furó I, 2009. Magnetic resonance imaging and nuclear magnetic resonance investigations of bentonite systems. SKB TR-09-27, Svensk Kärnbränslehantering AB.

Jansson M, 2009. Bentonite erosion. Laboratory studies. SKB TR-09-33, Svensk Kärnbränslehantering AB.

Neretnieks I, 2009. Some scoping erosion experiments in thin slits between glass plates. Report, Chemical Engineering, Royal Institute of Technology, KTH.

Neretnieks I, Liu L, Moreno L, 2009. Mechanisms and models for bentonite erosion. SKB TR-09-35, Svensk Kärnbränslehantering AB.